COMPRESSIONAL WAVE POWER SPECTRUM FROM SEISMIC SOURCES

Ilkka T. Noponen

Helsinki University

Prepared for:

Air Force Office of Scientific Research
Advanced Research Projects Agency

21 February 1975

AD-A008 961

Security Classification

DOCUMENT CONTROL DATA - R & D

(Security classification of title, body of abstract and indexing annotation must be entered when the overall report is classified)

1. ORIGINATING ACTIVITY (Corporate author) Institute of Seismology, Univ. of Helsinki Et. Hesperiankatu 4 SF-00100 Helsinki 10, Finland	2a. REPORT SECURITY CLASSIFICATION UNCLASSIFIED 2b. GROUP

3. REPORT TITLE

COMPRESSIONAL WAVE POWER SPECTRUM FROM SEISMIC SOURCES

4. DESCRIPTIVE NOTES (Type of report and inclusive dates)

Scientific. Final. 30 June 1972 - 31 December 1974

5. AUTHOR(S) (First name, middle initial, last name)

Ilkka T. Noponen

6. REPORT DATE 21 February 1975	7a. TOTAL NO. OF PAGES 70	7b. NO OF REFS 30
8a. CONTRACT OR GRANT NO AFOSR-72-2377 b. PROJECT NO. AO 2131 c. 62701D 2F10 d.	9a. ORIGINATOR'S REPORT NUMBER(S) ISBN 951-45-0538-7 9b. OTHER REPORT NO(S) (Any other numbers that may be assigned this report) AFOSR - TR - 75 - 0399	

10. DISTRIBUTION STATEMENT

Approved for public release; distribution unlimited

11. SUPPLEMENTARY NOTES TECH, OTHER	12. SPONSORING MILITARY ACTIVITY AFOSR (NP) 1400 Wilson Blvd. Arlington, VA 22209

13. ABSTRACT

The power spectra and waveforms of P-wave signals are studied using large aperture seismic array data. P-wave pulse lenghts and attenuation are determined by deconvolution of records to earth displacement, and by comparing spectral shapes with predictions from source models. A least-square procedure is used to fit predicted spectra to observations by varying model parameters. The attenuation parameter t on all ray paths from Asian locations to NORSAR studied was less than 0.4, having no correlation with distance and a regional variation. Larger attenuation is observed on ray paths from SW North America to NORSAR. P-wave pulse width is defined as ratio between pulse area and height. At magnitudes mb = 4.0, 5.0 and 6.0 the estimated mean pulse widths are 0.4, 0.65 and 1.1 seconds, and corresponding corner frequencies are 0.8, 0.5 and 0.3 hz, respectively. The RMS variation corresponds to a factor of 1.5. The explosion pulse widths have mean values 0.24 and 0.31 at mb = 5.0 and 6.0, respectively, with some disagreement in case of NTS shots. In a classification experiment using statistical limits derived from NORSAR data and pulse widths measured at LASA, classification capability intermediate between the "spectral" discriminant LTM and the mb-Ms discriminant was achieved, without any regional corrections.

PRICES SUBJECT TO CHANGE

DD FORM 1 NOV 68 1473

UNCLASSIFIED
Security Classification

Security Classification

14. KEY WORDS	LINK A		LINK B		LINK C	
	ROLE	WT	ROLE	WT	ROLE	WT
large seismic array						
seismic discrimination						
short period discriminants						
P-wave pulse width						
P-wave spectrum						
P-wave attenuation						
deconvolution						
seismic source duration						

Security Classification

February 21, 1975

FINAL SCIENTIFIC REPORT

COMPRESSIONAL WAVE POWER SPECTRUM FROM SEISMIC SOURCES

JUNE 30, 1972 - DECEMBER 31, 1975

ILKKA NOPONEN

Institute of Seismology, University of Helsinki
Et. Hesperiankatu 4, SF-00100 Helsinki 10
Finland

Approved for public release, distribution unlimited

SPONSORED BY

ADVANCED RESEARCH PROJECT AGENCY
ARPA ORDER No. AO 2131-1

ARPA Order No.: AO 2131-1

Program Code No.: 62701E 3F10 Project: AO 2131

Name of Grantee: University of Helsinki

Date of Grant: 72 JUN 30

Amount of Grant $22,640.00

Grant Number: OSR-72-2377

Grant Completion Date: 74 DEC 31

Project Scientist: Dr. Ilkka Noponen

Title of Grant: "SEISMIC WAVE PROPAGATION UNDER THE BALTIC SHIELD"

ISBN 951-45-0538-7

FOREWORD

The work reported in this document was performed at Institute of Seismology, University of Helsinki under the grant OSR-72-2377. The author spent several months at the Norwegian Seismic Array Data Center in Kjeller, Norway, and a month at the Seismic Discrimination Group in Lincoln Laboratory, M.I.T., Cambridge, benefiting from discussions with scientists and from use of special facilities at both places. Dr. Clint Frazier of Lincoln Laboratory gave to the author a useful algorithm.

ABSTRACT

The power spectra and waveforms of P-wave signals are studied using large aperture seismic array data. P-wave pulse lenghts and attenuation are determined by deconvolution of records to earth displacement, and by comparing spectral shapes with predictions from source models. A least-square procedure is used to fit predicted spectra to observations by varying model parameters. The attenuation on all ray paths from Asian locations to NORSAR studied was less than $t^*=0.4$, having no correlation with distance and a regional variation. Larger attenuation is observed on ray paths from SW North America to NORSAR. P-wave pulse width is defined as ratio between pulse area and height. At magnitudes m_b = 4.0, 5.0 and 6.0 the estimated mean pulse widths are 0.4, 0.65 and 1.1 seconds, and corresponding corner frequencies are 0.8, 0.5 and 0.3 hz, respectively. The RMS variation corresponds to a factor of 1.5. The explosion pulse widths have mean values 0.24 and 0.31 at m_b 5.0 and 6.0, respectively, with some disagreement in case of NTS shots. In a classification experiment using statistical limits derived from NORSAR data and pulse widths measured at LASA, classification capability intermediate between the "spectral" discriminant LTM and the m_b-M_s discriminant was achieved, without any regional corrections.

TABLE OF CONTENTS

LIST OF ILLUSTRATIONS

I. INTRODUCTION

In this second scientific report on study of P-waves observed by the NORSAR array, and on seismic event classification, the emphasis is on the determination of the lenght of the P-wave pulse from small-magnitude shallow events. The primary pulse from earthquakes[1] and from explosions[2] is rather generally accepted to be unidirectional, save a possible small overshoot of 10-20 % which is here usually disregarded. The lenght of the pulse is an attractive quantity from the point of view of discrimination, since it is so directly related to the physical properties of the source, and since it should not be so strongly influenced by variations in wave attenuation as third moment of frequency discriminants and other spectral discriminants measuring energy at high frequencies. We can expect the lenght of the wave pulse to be shorter for underground explosions than for earthquakes.

For example the source model by Randall[3] predicts modulation of P-wave amplitude spectrum, caused by the existence of two acceleration impulses, one at the initiation and the other at the stopping of the P pulse. In our study it was first tried to observe spectral modulation by cepstral methods[4]. The results were inconclusive, and for explosions we have the interfering pP echo. If we consider the detailed kinematic model of e.g. Savage[5] we find that several stopping phases are predicted, corresponding to various phases of rupture. Crustal responses may also produce modulation.

As described in this report, it is tried to return to the

original earth displacement wave pulse, since direct observation of the pulse seems the least ambiguous method. This requires correction for the NORSAR instrument response. If the pulse lenght is not too large, it is possible to get rather accurately back to the earth displacement even though the sensor has no D.C. response, as shown in next chapter. It seems also desirable to correct for some estimate of wave attenuation, made practical by Carpenter[6]. These corrections are made using an algorithm by Frazier[7]. As will be described, it turns out to be feasible to determine pulse lenghts from deconvolved records.

Source duration has usually been determined by spectral measurements, observing the high-frequency cut-off of a spectrum. This is a more statistical method than deconvolution to time domain, since by necessity it is as much or more a measurement on the P coda as on the primary pulse. We studied the spectra mainly to estimate wave attenuation, which is the dominating factor in spectrum at frequencies above 2-3 hz. The source spectral model variously called as omega-square (or omega-cube) by Aki[8], or the Brune model, or the spectral theory of seismic sources[9], is assumed. It is then necessary to know the corner frequency and the high-frequency asymptotic slope. These were determined from the data itself or assumed. The remaining spectral slope gives the attenuation. For the explosions, instead of the "Brune model", the spectral model of Haskell[2] with some later modifications was used. It will be here referred to by name "HSB-model".

Finally we use our observations on apparent source duration and wave attenuation in a classification experiment (chapter V) and for predicting values of two other discriminants (chapter VI).

II. MEASUREMENT OF PULSE AREA AND WIDTH

The teleseismic P-wave pulse is the derivative of the source time function (see chapter IV) and thus integration of the pulse can give information about the source. In particular the pulse area is proportional to the source seismic moment. Since the area under a function is equal to the value of its transform at the origin and the recording system has zero response at zero frequency, objections can be raised against the possibility of determination of pulse area. However, when the pulse width is so narrow that at the low-frequency end of the system pass-band it can be approximated by an impulse, its area can be determined. In spectral domain, it is not necessary to measure the power at zero frequency when determing the source seismic moment by spectral analysis. A measurement at any frequency situated within the flat power level surrounding the zero frequency (as predicted by the Brune theory) is sufficient.

The greater the pulse width, the closer to zero frequency one has to go for pulse area computation. Thus it is more easy to measure areas for short pulses than for long pulses.

In the following discussion, by system response is meant the combined effect of attenuation and seismograph response. The computation of these is, as mentioned in the introduction, based on the algorithm by Frazier[7].

Take S(f) to be the spectrum of earth movement. It is assumed to be the sum of seismic noise E(f) and of a transient P-wave

P(f). To study P(f) we want to compute an approximation $S_e(f)$ for S(f) from the spectrum T(f) of the recorded trace, which can written

$$T(f) = [E(f) + P(f)]R(f) + N(f) \tag{2.1}$$

where R(f) is the recording-system response and N(f) is the system noise. Dividing (2.1) by R(f) we get

$$S_e(f) = \left[E(f) + \frac{N(f)}{R(f)}\right] + P(f) \tag{2.2}$$

At f=0 R(f)=0, also at very small and large frequencies R(f) is small and N(f)/R(f) can become very large. It is necessary to limit estimation of $S_e(f)$ to some frequency band $f_L < f < f_H$.

The S/N ratio decreases as the range (f_L, f_H) is widened, for various reasons. A possible way to select values for f_L and f_H is to compute the time transform

$$S_e(t) = \int_{-f_H}^{-f_L} S_e(f)e^{i\omega t}\,df + \int_{f_L}^{f_H} S_e(f)e^{i\omega t}\,df \tag{2.3}$$

for various values of f_L and f_H and to select the widest range which gives acceptable S/N ratio on the resulting record. The limit f_H is not particularly critical because P(f) decreases rapidly at high frequencies. Cutting the spectrum at 5 hz did have little influence on our estimated P(t) but removed ringing problems. Selection of a suitable f_L is critical, however.

We represent the limits of integration in (2.3) by two rectangle functions $\Pi(x)$, subtracted from each other (figure II.1). The remainder function is

$$F(f) = \Pi\left(\frac{f}{2f_L}\right) - \Pi\left(\frac{f}{2f_H}\right) \tag{2.4}$$

with transform

$$F(t) = 2f_H \operatorname{sinc}(2f_H t) - 2f_L \operatorname{sinc}(2f_L t) \tag{2.5}$$

where $\operatorname{sinc}(x) = \sin(\pi x)/\pi x$. $F(t)$ is also shown in figure II.1. For illustration, values $f_L = 0.25$ hz, $f_H = 5$ hz were selected and the time function is shown as sampled with sampling rate 10 samples/sec.

The estimated earth motion spectrum becomes after multiplication with $F(f)$

$$S_e(f) = \Pi\left(\frac{f}{2f_H}\right) P(f) - \Pi\left(\frac{f}{2f_L}\right) P(f) + F(f)\left[E(f) + \frac{N(f)}{R(f)}\right] \tag{2.6}$$

It is now assumed that either f_H is equal to the Nyquist frequency or that approximately $P(f) = 0$ at $f > f_H$. Then the width of the main lobe of the function $\operatorname{sinc}(2f_H t)$ is smaller than our time resolving power or needs and the function can be approximated by an impulse $\delta(t)$. We then get for the time transform of $S_e(f)$

$$S_e(t) = 2f_H \delta(t) * P(t) - 2f_L \operatorname{sinc}(2f_L t) * P(t) + M(t) \tag{2.7}$$

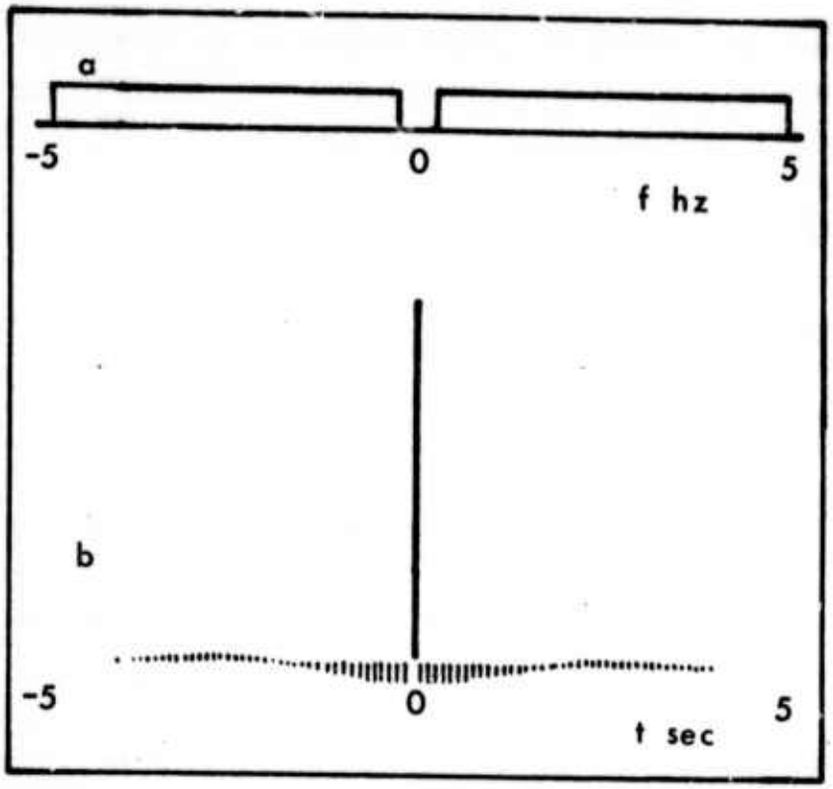

Fig. II.1. The filtering function F in frequency domain (a) and in time domain (b).

Fig. II.2. A schematical P-wave showing the onset (a) and end (b) of the P pulse.

where M(t) is the transform of the last (noise) term in (2.6).

As current theories of seismic sources predict, the pulse is assumed not to change sign. We take it to begin at t=a and to end at t=b. We want to determine the pulse area, ie. the integral of P(t) from a to b. Considering the convolutions in (2.7) and figure II.1 we may conclude that if

$$f_L << \frac{1}{b-a} < f_H$$

and noise and later reverberations can be disregarded, (2.3) gives the pulse shape, apart from a base line shift. Berckhemer and Burdick and Helmberger[10] used this condition to deconvolve long period seismograms from deep shocks.

A natural way to measure areas of short pulses when the base line is slowly drifting is to define the displacement at the moment of pulse onset as the base line level. It is then possible to relax the condition $f_L << (b-a)^{-1}$ to the less demanding condition $f_L < 0.35(b-a)^{-1}$, as will be shown below. Noise M(t) will now be disregarded, since it is stationary and uncorrelated with the signal its expected influence can be estimated from a noise sample.

Subtracting the amplitude $S_e(a)$ (the amplitude of $S_e(t)$ immediately before the pulse onset) from both sides of (2.7) and dividing by $2f_H$ we get

$$\frac{1}{2f_H}\left[S_e(t) - S_e(a)\right] = P(t) - D(t) \qquad (2.8)$$

where the "distortion term" D(t) is

$$D(t) = \frac{f_L}{f_H}\,\mathrm{sinc}(2f_L t) * P(t) - \frac{f_L}{f_H}\,\mathrm{sinc}(2f_L a) * P(a)$$

or

$$D(t) = \frac{f_L}{f_H}\int_a^b P(\tau)\left[\mathrm{sinc}(2f_L(t-\tau)) - \mathrm{sinc}(2f_L(a-\tau))\right]d\tau + \frac{f_L}{f_H}\int_b^\infty P(\tau)\left[\mathrm{sinc}(2f_L(t-\tau)) - \mathrm{sinc}(2f_L(a-\tau))\right]d\tau \qquad (2.9)$$

We investigate the first integral in (2.9), writing $D^I(t)$ for it. It is the contribution to $D(t)$ by the pulse itself. $P(t)$ is assumed to be positive in (a,b). If the pulse sign would be negative, (2.8) could be multiplied by -1.

Since t and τ are in (a,b) and

$$\mathrm{sinc}(2f_L(a-b)) \leq \mathrm{sinc}(2f_L(t-\tau)) \leq 1$$
$$\mathrm{sinc}(2f_L(a-b)) \leq \mathrm{sinc}(2f_L(a-\tau)) \leq 1$$

one can write

$$0 < D^I(t) < \frac{f_L}{f_H}\left[1 - \mathrm{sinc}\,2f_L(a-b)\right]\int_a^b P(\tau)\,d\tau \qquad (2.10)$$

Thus the error caused by the term $D^I(t)$ in the determination of pulse area can be estimated from (2.10) as

$$0 < \int_a^b D^I(t)\,dt < \frac{f_L}{f_H}(b-a)\left[1 - \mathrm{sinc}\,2f_L(a-b)\right]\cdot \int_a^b P(\tau)\,d\tau \qquad (2.11)$$

The upper limit of the estimate (2.11) for areal distortion is plotted to figure II.3 as a function of the ratio between the cutoff period $T_L = 1/f_L$ and the pulse base lenght b-a.

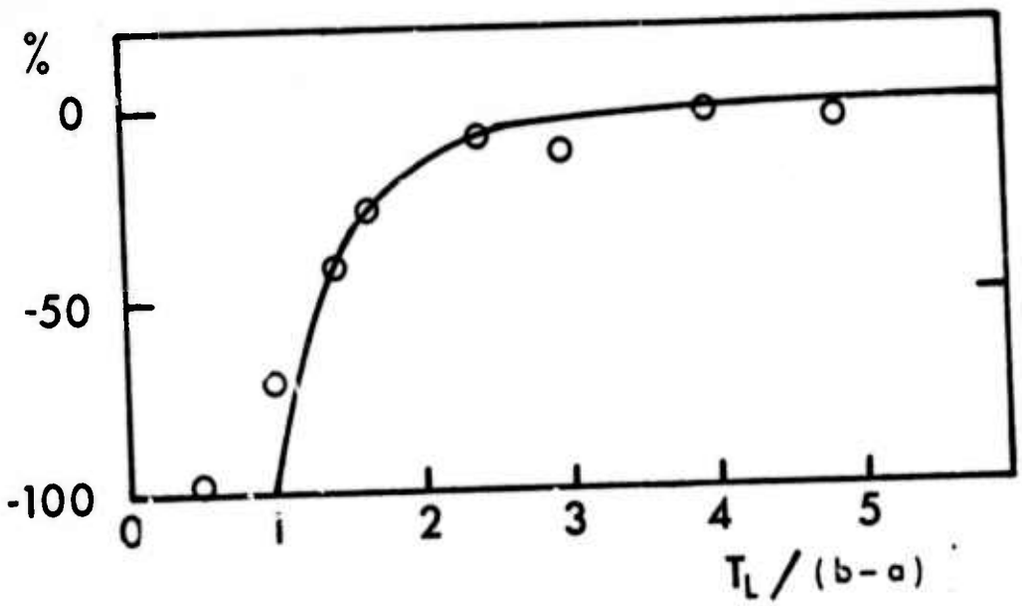

Fig. II.3. The predicted maximum distortion of measured pulse area as a function of the ratio between cutoff period and pulse duration (the line) and observed pulse area distortion (the circles).

The pulse area distortion was tested in the case of an event with a simple pulse-like P-waveform and a good S/N ratio. Deconvolved records with various values of f_L are shown figure II.4. The value f_H=5 hz is used and the attenuation amounting to t^*=0.3 has been corrected for.

The event occurred at April 11, 1968, 06-46-27.4 under the Japan Sea at depth 511 km. Magnitude m_b is 5.0. The width b-a of the pulse base is determined as 1.04 s from the low f_L records. The per cent reduction in pulse area, relative to the area determined with f_L=0.1 hz, is shown in figure II.3 as a function of $f_L^{-1}(b-a)^{-1}$. Reduction of pulse area follows closely the limit predicted by (2.11). Overstepping may be caused by measurement inaccuracies. The cut-off at

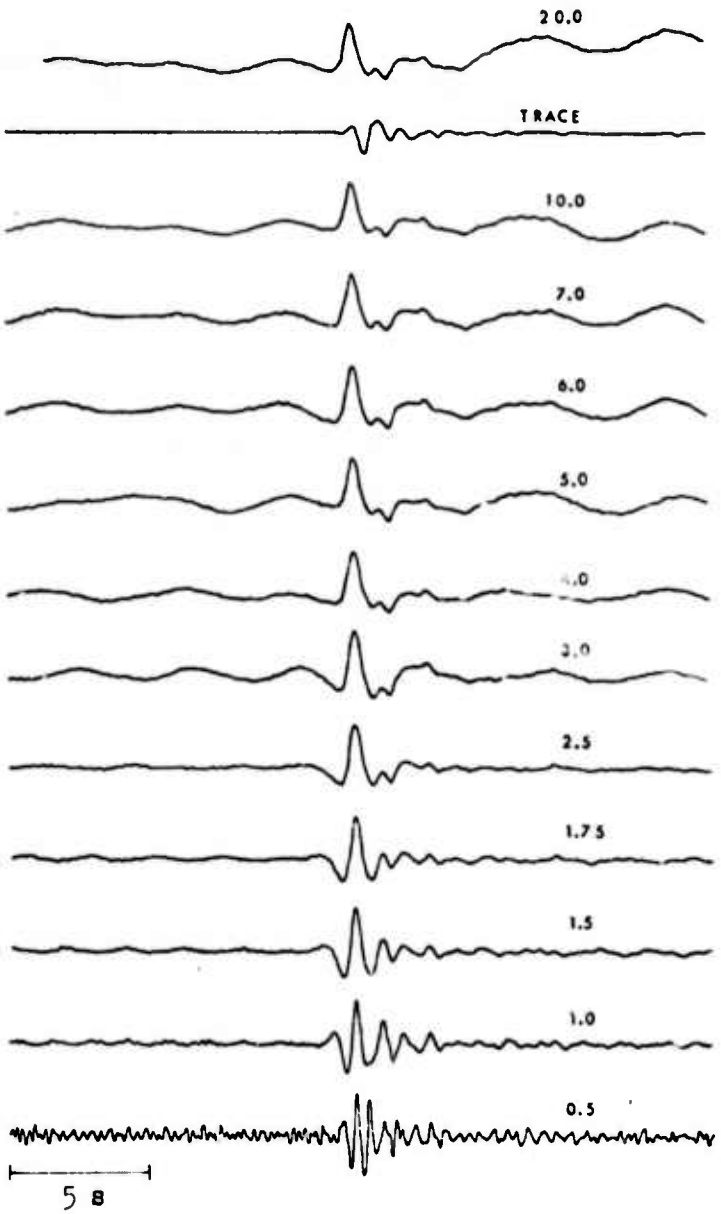

Fig. II.4. A P-wave record from a deep event under Japan Sea deconvolved using several different long-period cut-offs, shown at the right margin. The original trace is second from top. Note the development of a precursor with decreasing cut-off period, and the stability of shape at the long cut-offs.

f_L was not quite abrupt, tapering was used. However, the discussion applies to any function with transform roughly of the sinc(x) form.

We have not yet discussed the second integral of (9). One can give estimates for it, but the distortion due to later reverberations may or may not be present, and may be of either sign. The distortion caused by the pulse itself is, on the contrary, always present and always decreases the pulse area. It is thus of more fundamental and important nature.

The width of the pulse is defined as the ratio area/maximum amplitude, which is a standard definition. The maximum amplitude is also measured relative to $S_e(a)$. The implicit distortion on the pulse amplitude by $D^I(t)$ term is given limits in (2.10). Because both of the pulse area and its maximum amplitude are reduced by the term $D^I(t)$, the change in their ratio should be relatively less than the change in area. Figure II.5 shows the apparent pulse area and width as a function of the cut-off period/pulse width ratio. The area and width are plotted relative to the area and width obtained using cut-off 10 seconds. The width is less distorted by the cut-off than the area, as suggested above.

An empirical rule-of-thumb which arose from deconvolving a number of events was that if T_L/W (cut-off period/true pulse width ratio) is greater than 8, pulse area and shape remain unchanged, if $8 < T_L/W < 4$ pulse width is unchanged but a precursor appears, if $4 < T_L/W < 2$ the pulse width is reduced by the cut-off, and if $T_L/W < 2$ no measurement is possible. Since W is typically about half of the pulse

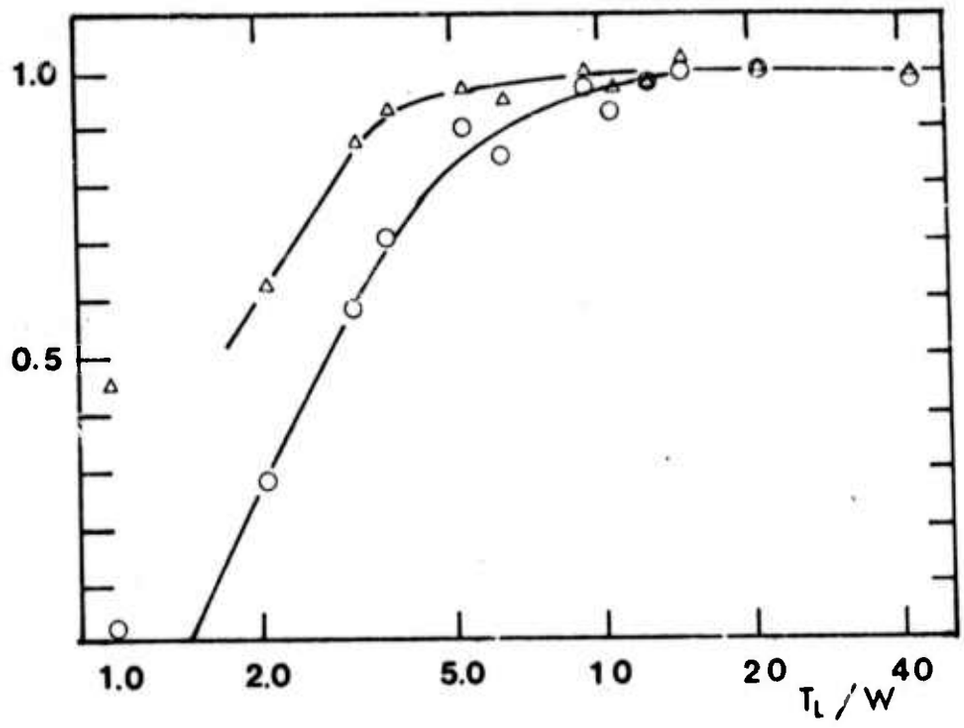

Fig. II.5. Measured pulse width (triangles) and pulse area (circles) of the Japan Sea deep shock, as a function of the cut-off period/true pulse width ratio. Both quantities are shown relative to their values measured with cut-off 10 seconds.

duration b-a, these are in agreement with the other results of this chapter. A corollary of this is that if the measured pulse width is less than a fourth of the cut-off period, we can be rather confident that no distortion has occured. If the measured pulse width is greater than that limit, apparently what we can say is that the true pulse width is greater than our measured value, a statement which frequently is rather useful.

Deconvolution of signals from explosions in Western Russia, at distances less than 30 degrees from NORSAR, gave usually

different results than those from more distant explosions. Instead of the simple waveform from distant explosions we often observed complicated and elongated low-frequency oscillations and in some cases dilatations of the first motion. Our conclusion is that the pulse width measurement by deconvolution cannot be applied at $\Delta < 30^{o}$ because of multipathing in the upper mantle (for multipathing, see e.g. figure 6 of reference 11).

The measured pulse width is influenced by the amount of attenuation corrected for in the deconvolution. This was investigated by deconvolving a few events with several different t^{*} values. Results are shown in figure II.6.

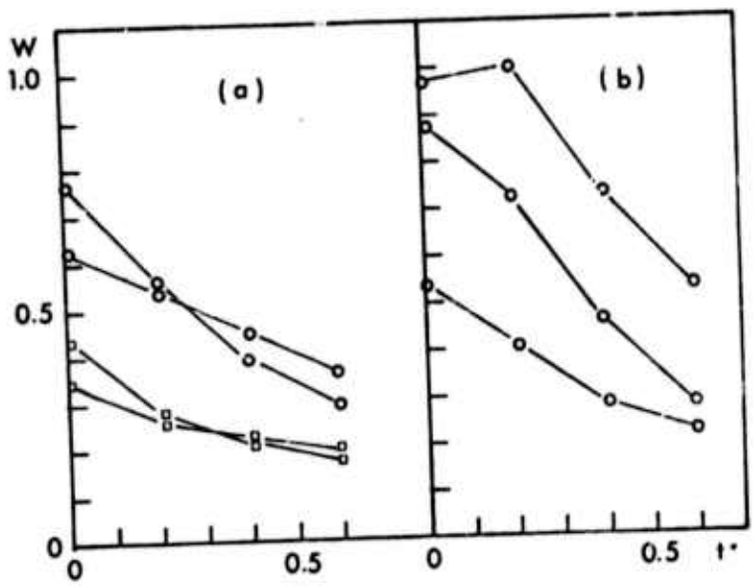

Fig. II.6. Pulse widths measured for explosions (a) and earthquakes (b) after deconvolution with various values of assumed t^{*}. Events are recorded at NORSAR. Circles denote two NTS explosions, squares denote two E. Kazakh shots.

When the used t^* value is increased from 0.2 to 0.4, the pulse width decreases by 20-30 %. According to these few examples, for accurate determination of pulse width an accuracy of 0.1 in t^* estimates is sufficient, and if we are willing to accept errors up to 50 % the value of t^* has no significance, as long as it is less than 0.6, which we believe to be true.

III. MEASUREMENT OF P-WAVE ATTENUATION

Parallerly with measurements in time domain, observations in the spectral domain were done. Power spectral measurements are of more statistical nature than direct measurements on a pulse. In using the short period sensor data for spectral studies on P-waves from events in the magnitude range 4.0 - 6.0 (m_b), one cannot avoid the influence of the anelastic attenuation, since the observed frequency range extends above 4 hz. It is tried to turn this difficulty into a benefit by including the attenuation factor $\exp(-\pi f t^*)$, t^* as a free parameter, into the spectral model which is fitted into data, in the hope of mapping attenuation on various wave paths.

The procedure for measuring the response-corrected P-wave spectra from NORSAR data was described in the 1st Scientific Report[12], and will not be repeated here. The average noise-corrected power spectrum of NORSAR subarray beams is used.

We are employing the common spectral model discussed by Randall[9], and proposed by Haskell[13], by Aki[8] and by Brune[14]. Including the attenuation factor it predicts spectral amplitudes

$$|A(f)| = \frac{A_o \exp(-\pi f t^*)}{1 + (f/f_o)^n} \qquad (3.1)$$

where A_o is a factor independent of frequency. f_o is the corner frequency, usually associated with source dimension. Both of the factors $\exp(-\pi f t^*)$ and $(1 + f^n f_o^{-n})$ cause the amplitude to decrease with increasing frequency.

If we have available spectral information from frequencies sufficiently higher than the corner frequency, these two factors can be separated from each other. When studying some frequency range, we can always determine the level and slope of the spectrum. In a log amplitude/linear frequency plot the slope is

$$\frac{d(\log|A|)}{df} = - \frac{n}{f(f_o{}^n f^{-n} + 1)} - \pi t^* \qquad (3.2)$$

Even assuming a value for n we cannot from the slope determine t^* independently from f_o. But if the frequency range is sufficient that we can observe the systematic change in slope, which multiplied by f^2 is

$$f^2 \frac{d^2(\log|A|)}{df^2} = \frac{(n-1)n}{\frac{f_o{}^n}{f^n} + 1} \qquad (3.3)$$

then by fixing n we can determine f_o, and then t^* from (3.2).

The existence of modulation in P-wave spectra makes it necessary to observe a so wide frequency range to estimate the derivatives (3.2) and (3.3), that they cannot any more be described by single average numbers. Therefore the model (3.1) was rather fitted to the logarithm of the observed spectra by an iterative least-squares procedure. However we would note that under conditions $f >> f_o$ (3.2) and (3.3) become

$$f \frac{d(\log|A|)}{df} = - n - \pi t^* f \qquad (3.4)$$

$$f^2 \frac{d^2(\log|A|)}{df} = (n-1)n \qquad (3.5)$$

When the line described by (3.4) was fitted to the spectral derivative of 11 earthquakes in Central Asia in the frequency range 0.63 - 5.78 hz, average values n = 1.75 +- 0.40 and t^* = 0.24 +- 0.03 s came out. The condition $f \gg f_o$ was not well fulfilled, however the result for t^* compares rather well with those described below.

Going now to describe the results from the iterative least-squares model fitting, the parameters determined in the procedure were $\log(A_o)$, $\log(f_o)$ and t^*. The parameter n was assigned values 2 and 3. Spectra from several events from a same region were inverted simultaneously, keeping t^* a common parameter for all these shocks. To summarize, for each region the model was made to fit observations from j events, each having spectral estimates at i frequencies. By inversion of ij equations, the parameters $t^*, f_{o(1)}, \ldots, f_{o(j)}, A_{o(1)}, \ldots, A_{o(j)}$ were determined.

The most probable values for n are 2 and 3. Recently, Savage[15] suggested the value 2.5 for a circular fault with a rupture spreading at subsonic velocity, and where the slip at any point builds up gradually. All detailed models on body waves generated by a deterministic fault rupture predict oscillations in the spectrum. A smooth spectrum is however useful as an approximate model. We are here allowing for only one corner frequency. This is to be understood as an approximation for the case where the different corner frequencies are not too far separated. E.g. the slip time function produces a corner

frequency in addition to the corner frequency associated with rupture duration. At each corner frequency the exponent n is decreased by one[16].

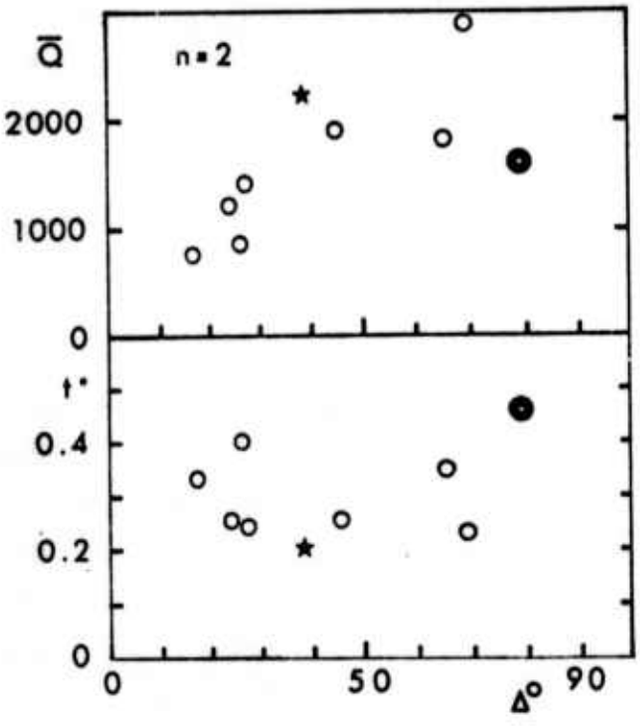

Fig. III.1. Estimated attenuation as a function of distance, when the model parameter n=2. Filled and open circles denote ray paths from North America and Asia to NORSAR, respectively. The asterisk denotes the path from E. Kazakh test site to NORSAR.

Values of t^* and of mean Q estimated by model fitting with n=2 are shown in figure III.1. The corresponding results with value n=3 are shown in figure III.2. Both results are shown in table III.1. In neither of the figures the attenuation appears as a simple function of distance. This is not due to inaccuracy of measurement, the average spectral slopes at high frequencies are systematically different

between such event groups as Sakhalin and Kuriles, or Greece and Turkey (see also the plots in ch. III of ref. 12). There are only two explanations for this, one is that the earthquake processes at the compared regions are radically different, or that the attenuation is different on the respective ray paths. The latter explanation is much simpler and causes for attenuation differences are not difficult to find from regional tectonics.

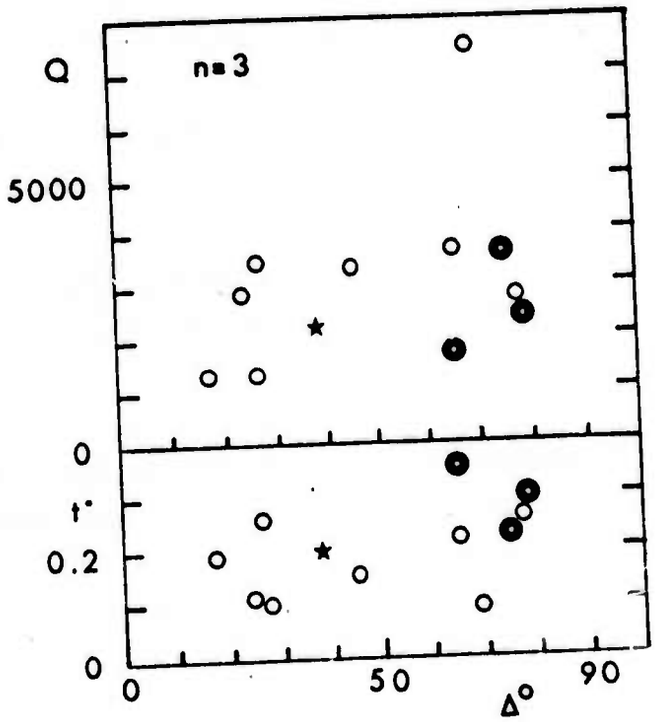

Fig. III.2. Estimated attenuation on ray paths as a function of propagation distance, with spectral model parameter n=3. Filled and open circles and the asterisk denote ray paths from western North America, Asia and Eastern Kazakh to NORSAR, respectively. Explosions and earthquakes were fitted with different models.

A further check was made on the t^* values. To all observed earthquake $\log_{10} f_o$'s were fitted a least square line, giving

expected $\log_{10} f_o(m_b)$. For each region was then separately computed the mean deviation

$$d = \text{AVE}[\text{OBS}(\log_{10} f_o) - \text{EXP}(\log_{10} f_o)]$$

Now, if the variations in t^* would be caused by the instability of inversion, such that a decrease in t^* is offset by a decrease in f_o and vice versa, we would expect to have a positive correlation between d and t^* among the different regions. On the contrary there exists a negative correlation between the two quantities. This can again mean two things. Either the corner frequencies are systematically higher at such regions from where the ray paths to NORSAR have a high Q, or, more probably, our spectral model does not quite well describe the reality. This unexpected correlation is observed both for the cases n=2 and n=3.

The RMS scatter of corner frequencies around the least squares line is less for the case n=3 than for the case n=2, by a factor of two. On the other hand, the range of t^* values in the case n=2 agrees better with the observations by Frazier and Filson[17] and Noponen (fig. III.13 of ref. 12). When spectra from LP instruments were included in data, the RMS values in model fitting increased (events in Central Asia and W. coast of N. America). This is natural and does not mean that the results would be less reliable, on the contrary the wider frequency range gives more reliable results. Some data is shown with fitted models in figure III.3.

The spectral model ("HSB-model") given by von Seggern and Blandford[18]

Table III.1. Results of t^* estimations for different regions. N=number of events, Δ=distance, σ=standard deviation of t^*, 10^d=factor indicating how much regional f_o average deviates from total average, parenthesis indicate that the factor is not significantly different from 1.0 (see text), RMS=scatter around fitted spectral models (in dB), $\bar{Q}$=mean Q computed from t^*.

REGION	N	Δ	$\bar{\Delta}$	t^*	σ	10^d	RMS	$\bar{Q}$	t^*	σ	10^d	RMS	$\bar{Q}$
				n=2					n=3				
SAKHALIN	19	65-66	65	.35	.01	(0.8)	1.7	1800	.21	.01	(0.95)	1.8	3100
KURILES	12	69-69	69	.23	.02	2.0	1.4	2900	.09	.02	1.5	1.4	7400
SOUTH OF HONSHU	5	77-77	77	no convergence					(.26	.03	1.5	1.6	2700)
CENTRAL ASIA	15	37-56	45	.26	.01	(1.0)	2.8	1900	.15	.01	(1.1)	3.0	3300
CRIMEA-CAUCASUS	3	22-30	27	.24	.05	(2.0)	2.2	1400	.10	.04	(1.3)	2.1	3400
GREECE	14	20-28	24	.26	.01	(1.0)	1.5	1200	.11	.01	(1.0)	1.7	2800
TURKEY	8	23-30	26	.40	.01	(0.8)	1.3	840	.26	.02	0.9	1.6	1300
ITALY	4	16-18	17	.33	.01	0.35	1.3	730	.19	.01	0.7	1.2	1300
WEST COAST OF NORTH AMERICA	6	65-83	75	no convergence					.23	.02	0.6	4.3	3100
VANCOUVER ISL. REG.	2	65-65	65	not computed					.36	.07	0.5	4.1	1800
GULF OF CALIFORNIA	5	79-79	79	.46	.02	0.5	1.0	1600	.30	.02	0.7	1.0	2400
EASTERN KAZAKH[1]	8	38-38	38	.20	.01	2.0	2.4	2205	.20	.01	1.7	2.4	2205

1) The explosions at E. Kazakh have been fitted with a different model. The same results are written to both of the columns n=2, n=3.

$$|A(f)| = \frac{A_o\left[(2B+1)^2 \left(\frac{f}{f_o}\right)^2 + 1\right]^{\frac{1}{2}}}{\left[\left(\frac{f}{f_o}\right)^2 + 1\right]^{\frac{3}{2}}} \qquad (3.6)$$

was fitted to the observed spectra from 8 E. Kazakh shots, using value B=2. The observed t^* is 0.20 and the resulting corner frequencies seem reasonable. Observed and fitted spectra are shown in fig. III.4. The success in fit was apparently caused by the wide frequency range (up to 6 hz) allowed by the small attenuation and use of 20 hz sampling rate. Analysis of other explosion regions where high attenuation (NTS-NORSAR) or our use of data from event tapes with 10 hz sampling rate limited the frequency range to 3 hz, gave corner frequencies smaller than those observed for earthquakes, together with relatively low t^* values. The reason is probably the strong modulation of spectrum by the pP phase, requiring a wide frequency range in the estimation of the general trend of spectrum. Direct comparison between NTS and E. Kazakh explosion spectra recorded at NORSAR leaves no doubt of the much stronger attenuation on the NTS-NORSAR path, the suggested difference being about 0.28 in t^* (figure III.5).

If we add 0.28 to the absolute t^* value determined for the E. Kazakh-NORSAR path, we get 0.48 as the absolute t^* on NTS-NORSAR path, in a reasonable agreement with the value 0.41 obtained by Filson and Frazier[17].

A further experiment was to compute the average spectrum of 4 NTS shots with mean m_b=5.2, and the average spectrum of 6 E. Kazakh shots with mean m_b=5.5, to restrict the corner

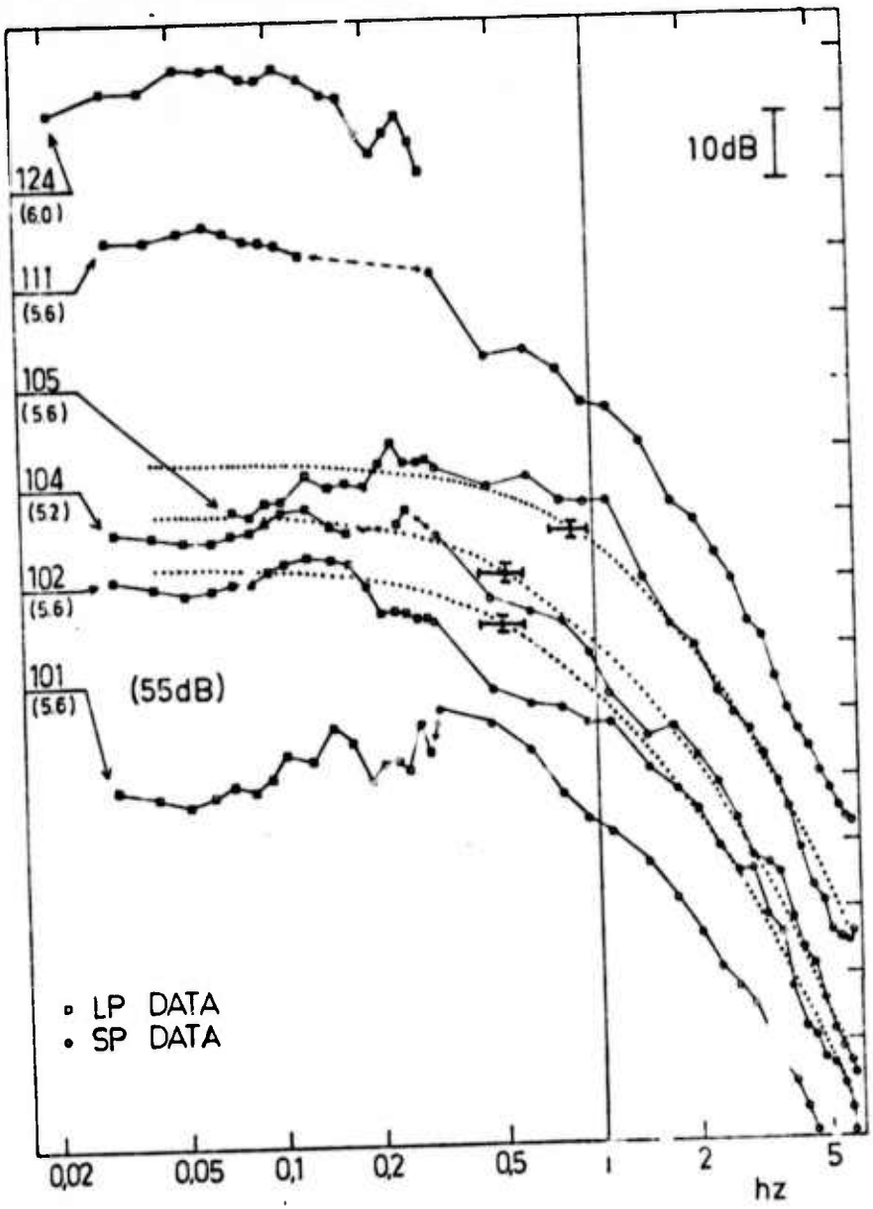

Fig. III.3. Observed spectra from a few earthquakes in Central Asia, together with spectra predicted by the Brune model, fitted into the observations by varying parameters in several least-squares iterations. The crosses at the center indicate the position of f_o and the standard deviations of f_o and A_o, for each curve.

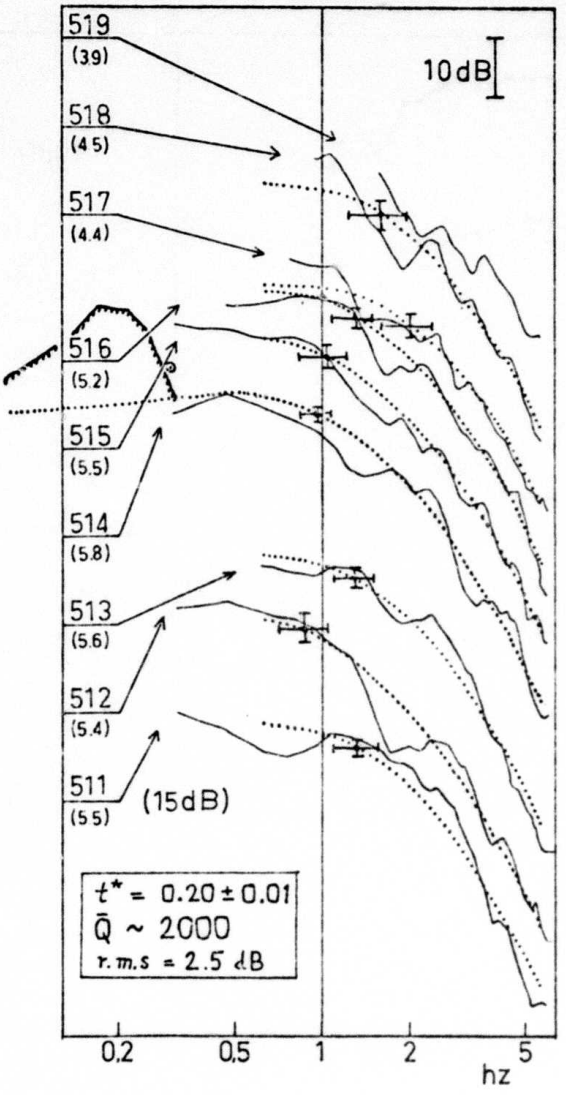

Fig. III.4. Observed spectra from E. Kazakh explosions, together with spectra predicted by the Haskell - von Seggern - Blandford model fitted into observations by varying parameters in successive least-squares iterations. The crosses close to 1 hz indicate the position of f_o and the standard deviations of f_o and A_o, for each model curve.

frequencies of the two average spectra as equal, and to determine the one f_o and the two t^* in a simultaneous inversion to the HSB-model. Results are given in table III.2.

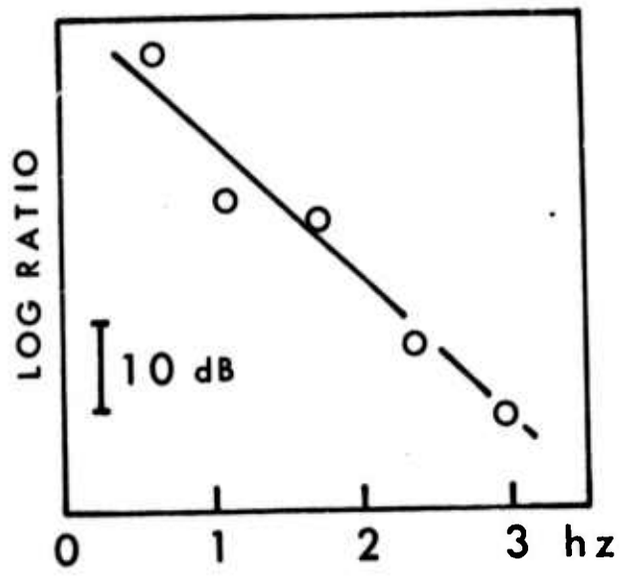

Fig. III.5. Spectral ratio between NTS and E. Kazakh explosions in the magnitude range (m_b) 5.0-6.0. Assumption of similar average source spectrum gives for attenuation difference between paths NTS-NORSAR and E. Kazakh-NORSAR the value $t^*=0.28$, from the visually fitted line in the figure. This figure is in agreement with the attenuation difference between southwestern North America - NORSAR and Central Asia - NORSAR paths, determined from the ratio of earthquake spectra[12] as 0.279 ± 0.004.

Table III.2 results of an inversion experiment.

t^*(NTS-NORSAR)	0.403 ± 0.076
t^*(E. Kazakh-NORSAR)	0.150 ± 0.027
The common f_o	0.61 ± 0.25 hz
RMS	2.5 dB

and the observed and predicted spectra are shown in figure III.6. In averaging spectra from different shots the effect of the pP modulation probably decreased, and the high-frequency E. Kazakh spectra stabilized the common solution. The impression from the figure is that the lowest frequency band in the NTS spectral average has a disproportionally high amplitude, distorting the solution so that the common f_o approaches the earthquake f_o at a similar magnitude.

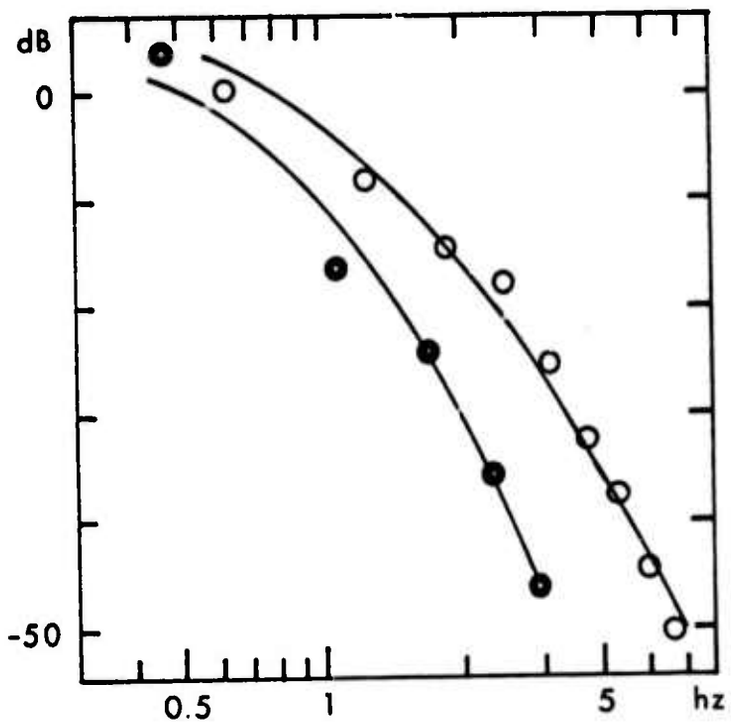

Fig. III.6. Average spectra for 4 NTS explosions (filled circles) and 6 E. Kazakh explosions (open circles) and HSB model spectra simultaneously fitted to both data. The dB scale is relative to the zero-frequency level of the theoretical curves.

IV. DURATION OF EARTHQUAKE AND EXPLOSION SOURCES

At this stage no interpretation of the observations in terms of a finite source model will be done. Only the apparent source time function S(t) will be discussed. If a point source consisting of force couples is assumed, S(t) becomes the time history of the forces, the radiated teleseismic P-wave being the derivative dS(t)/dt. The difference between earthquakes and explosions lies then only in the geometry of the force couples, a double force couple describing the earthquake source[19], three perpendicular couples without moment the explosion source[20].

A point source is in principle an unsuitable model, since the wavelenghts of the observed waves are of the order of earthquake size. However, since our observations for each shock are limited to a single direction, there will be no need to use finite source models giving different S(t) to different directions.

As S(t) is monotonous[1,21], save for a possible small overshoot[2] which we disregard here, the observations in time domain and frequency domain can be conveniently related through the reciprocal concepts of spectral width and pulse width[8]. Defining the width of a function as

$$W = \frac{\int_{-\infty}^{\infty} F(s)\, ds}{F(o)} \qquad (4.1)$$

we get for the width of the amplitude spectrum of the Brune

model the value πf_o, and for the corresponding model with the high-frequency spectrum proportional to f^{-3} the value $3^{-1/2}\pi f_o$. If the pulse shape in time domain is an even function the pulse width is the inverse of the spectral width. Thus the relationships between the pulse width W_p and the corner frequency are

$$W_p = \frac{1}{\pi f_o} \tag{4.2}$$

$$W_p = \frac{\sqrt{3}}{\pi f_o} \tag{4.3}$$

for the values n=2 and n=3, respectively.

Pulse width measurements, made by the methods described in chapters II and V, are plotted in figure IV.1 against the corner frequencies measured as described in chapter III, for the same events. Results from both of the assumptions n=2 and n=3 are shown. Only events with distance from NORSAR greater than 30 degrees are included.

When comparing the lines predicted by (4.2) and (4.3) to the plotted data, one observes than in case of n=2 about 2/3 of the points fall reasonably close to the prediction. Among the 1/3 which have f_o over twice the value predicted from the pulse width we find all of the 7 plotted Kuriles shocks, 4 of the 19 Sakhalin shocks and 3 of the 14 Central Asia shocks. In case of n=3 such spurious high frequencies do appear only for a few of shocks.

At least a couple of explanations suggest themselves. In chapter III it was noticed that for the ray paths with high

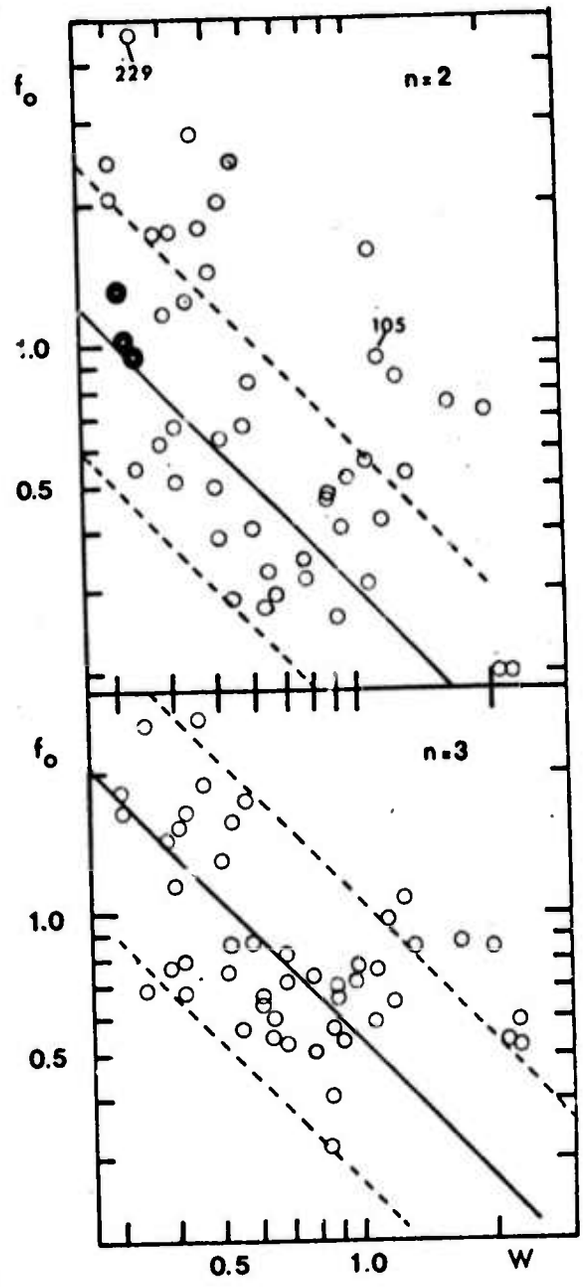

Fig. IV.1. Measured corner frequencies plotted against the measured pulse widths for the two cases n=2 and n=3. The continuous lines show the expected relations. Filled circles denote E. Kazakh explosions.

t^* values also the corner frequencies were above average. It was then suggested that either the attenuation model or the source spectral model is not accurately describing the reality, causing a coupling between the parameters t^* and f_o. This could explain why all the Kuriles shocks have excessive f_o when n=2. We can also have a, say, f^{-1} asymptotic spectral dependence up to a fairly high second corner frequency in case of some events. This seems to apply to the event "229" in Central Asia, for which the spectral slope turns normal around 4 hz. The pulse lenght needs not then to be particularly short, but the pulse has "sharp corners". In case of the event "105" we have <u>after</u> the primary pulse (with duration 1.4 s and width 1.1 s) a large-amplitude oscillation with frequency 1 hz, which probably produces the sharp corner observed in spectrum at 1 hz (spectrum shown in reference 12, fig. II.1). Such later reverberations can be caused by a thick low-velocity layer above a shallow source[22].

We make a preliminary assumption that the high corner frequencies which disagree with corresponding pulse widths are a result of our crude source spectral model not always being able to model the spectrum correctly, and that they need not imply very short widths for the primary pulse.

In figure IV.2 the 90 % confidence limits for the <u>true</u> pulse width[23] from various sets of data are shown as functions of m_b. The following assumptions have been made: the width/magnitude relationship is roughly linear in the magnitude interval of study, the individual width measurements are distributed randomly and roughly normally around the parent width/m_b line, the measured corner frezuencies can be transformed to pulse widths by (4.2) and (4.3), and the errors in

magnitude are much smaller than the scatter in pulse width.

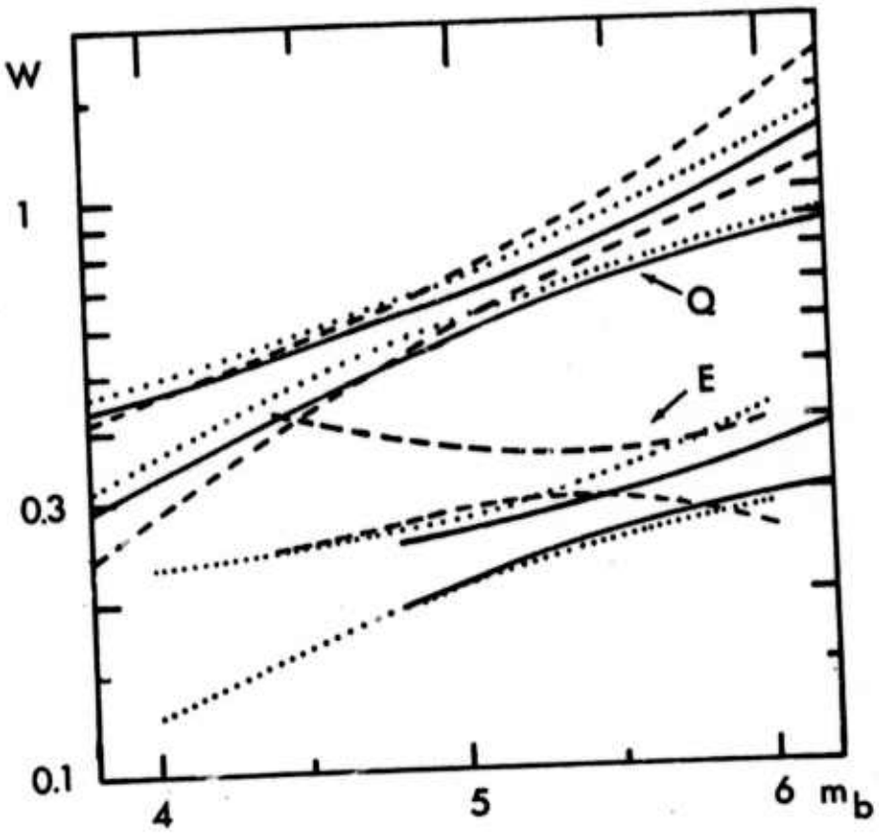

Fig. IV.2. The 90 % confidence limits for true pulse width as a function of magnitude, deduced from various sets of data for earthquakes (the upper curves marked with Q) and for explosions (the lower curves marked with E). Limits drawn with dotted lines are derived from corner frequency measurements, the other limits are from direct measurements on pulse width.

The different samples which are described by fig. IV.2 are: (1) Corner frequencies measured under assumption n=3 from spectra of 91 earthquakes recorded at NORSAR, and transformed to pulse widths by (4.3). The m_b range is 4.1 to 6.0, limits are plotted by dotted line. (2) Pulse widths measured from deconvolved NORSAR records of 53 earthquakes, forming a subset of previous the set. Magnitude range is 4.1 to 6.0, limits are plotted by broken line. (3) Pulse widths measured from deconvolved LASA records of 59 earthquakes[24], in magnitude range 4.1 - 6.1. Limits are plotted by continuous line. (4) Corner frequencies measured using the HSB-model from spectra of 8 E. Kazakh explosions recorded at NORSAR. The magnitude range is 4.2 - 5.8, limits are plotted with dotted line. (5) Pulse widths measured from deconvolved NORSAR records of 22 explosions in Kazakh and NTS. Magnitude range is 4.4 to 5.8, limits are plotted with broken line. (6) Pulse widths measured from deconvolved LASA records of 10 explosions at various locations[24], the magnitude range is 4.8 to 6.1. Limits are plotted with continuous lines.

Figure IV.3 seems to give a consistent picture of the P-wave pulse width and its change with magnitude for earthquakes. For the explosions there is a disagreement between the data sets (5) and (6), at magnitudes below 5.5. It does not seem difficult to clarify the situation with further research.

Of more interest from the point of view of study of earthquake mechanism would be the plot of pulse width against source seismic moment, which can be computed from the pulse area. Such a plot will however be worse as an identification diagram, due to the small moments of explosions. The seismic moments could also be plotted against the magnitude m_b, giving

a picture resembling the m_b/M_s plot, since at $m_b \leq 6$ M_s is proportional to the moment[25]. The influence of source depth would be removed, however, and the influence of source mechanism would be different. A preliminary plot showed that a moment/m_b plot gave no better discrimination than a width/m_b plot.

The union and intersection of the confidence regions of figure IV.2 are shown in figure IV.3 by the hatched and black regions, respectively. Earthquakes and explosions are treated separately. The confidence limits computed from the f_o derived under assumption n=2 are also shown, by broken lines. The region bounded by these limits has an intermediate position between the explosion and earthquake 90 % confidence regions derived from the other sets of data. As mentioned above, our assumption was that spurious high corner frequencies have distorted the average properties of this set of data.

Comments on NTS explosions. Even after taking account the large attenuation on the ray path NTS-NORSAR, the pulse widths of NTS explosions seem systematically somewhat larger than those of the Eastern and Central Kazakh explosions, e.g. causing the disagreement between the data sets (5) and (6). One explanation for this could be that on the frequency 1.3 hz, around which the m_b is measured, an attenuation difference of .28 in t^* produces a factor of 3 difference in spectral amplitude. This rough calculation suggests that for two explosions of similar yield fired under similar conditions at the two sited, the NTS explosion would be given up to 0.5 units smaller magnitude than for the E. Kazakh explosion, at NORSAR. If the attenuation conditions on ray paths from the two sites to the majority of the stations are similarly

different than on paths to NORSAR, the NTS explosion magnitudes should be corrected upwards by some source factor, for comparison. The disagreement between Kazakh and NTS pulse widths would then decrease.

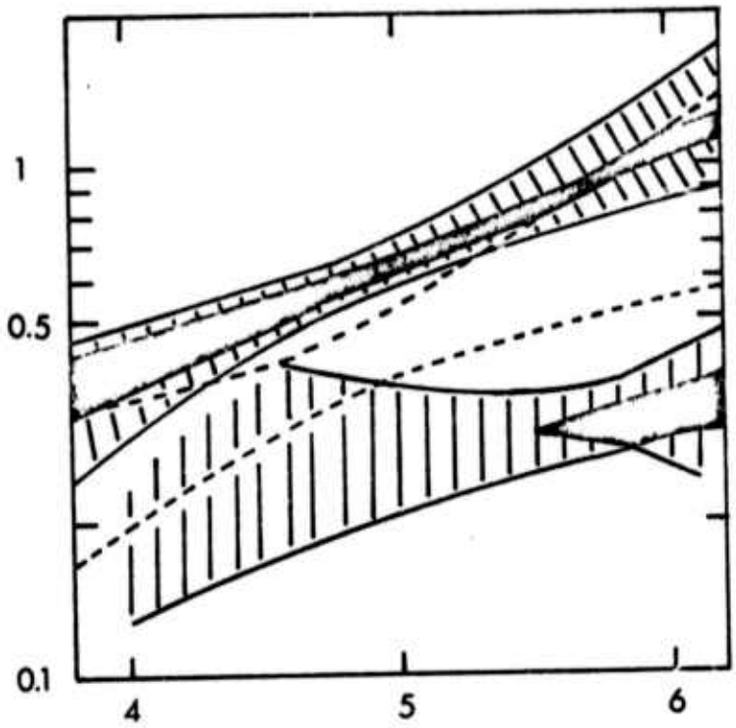

Fig. IV.3. The union (hatched) and intersection (black) of the confidence regions shown in previous figure, separately for earthquakes and explosions. The confidence limits for an earthquake set analysed in spectral domain under assumption n=2 are shown by broken lines. Our interpretation is that they are distorted by spurious high corner frequencies.

Figure III.6 suggests excessive low frequency energy for E. Kazakh explosions. In deconvolving the NTS records from NORSAR, sometimes slow motions of large amplitude were observed. We cannot give any explanation for them, we are not even sure of their reality. But inevitably they distort our spectral measurements. In figure IV.4 are shown the NORSAR beam record and deconvolutions with cut-offs 10 and 2.3 seconds for the NTS explosion on day 156 of 1973, time 17-11-32.5, displaying a large later pulse with duration of appr. 4 seconds.

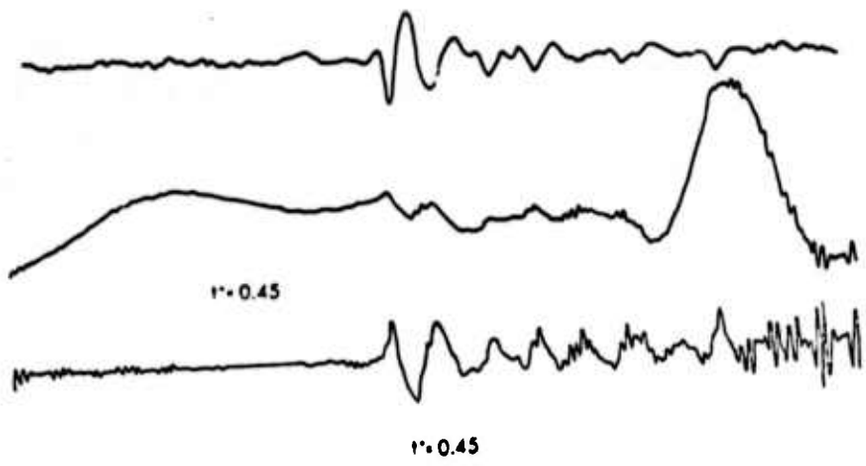

Fig. IV.4. NORSAR beam trace (top) of a NTS explosion, its deconvolution with cut-off 10 seconds and with cut-off 2.3 seconds (bottom).

V. CLASSIFICATION EXPERIMENT USING PULSE WIDTH

The pulse width determination method developed using the NORSAR data was tried on a set of data collected by Lacoss[24] from LASA records on 1966-1968. It was possible for the author to use the console system of the Seismic discrimination group in Lincoln Laboratory, M.I.T. The system was well suited for this kind of analysis and speeded up the work. The procedure followed is now described:

(1) The LASA beam record was displayed on the screen and by varying the gain, the onset time and polarity were observed.

(2) The beam was deconvolved with $t^*=0.3$ s and using low-frequency cut-off periods of 10, 7, 4, 2.5 and 1.75 sec. The resulting five traces were displayed on the screen.

(3) Generally the S/N ratio decreases with increasing cut-off period. The trace with longest cut-off period and with acceptable S/N ratio was selected. It was checked that the pulse had a correct polarity and began appr. 0.3 seconds prior to the onset on beam. If no sufficient S/N ratio was observed or there was a disagreement in pulse onset time or polarity with the beam record, the event was usually placed to the category of non-measurable events.

(4) The pulse width was measured semi-automatically.

Two positions were manually defined on the selected trace. The first, t_1, was the expected onset time on deconvolved record, the second, t_2, was approximately on the pulse maximum. Then an integration procedure was triggered, giving the pulse width as

$$W = \frac{\int_{t_s}^{t_e} [A(t) - A(t_s)]\, dt}{A_m - A(t_s)} \qquad (5.1)$$

where t_s is the point where min $A(t) | t_1 \leq t < t_2$ is observed. t_e is $\min(t_a, t_b)$, where t_a is the first point where $A(t) < A(t_s)$ and $t > t_2$, and t_b is the first point where $dA(t)/dt > 0$, $t > t_2$ and $A(t) < 0.3(\max A(\tau) | t_s < \tau < t)$. $A_m = \max A(t) | t_s < t < t_e$.

In figure V.1 deconvolved records of a magnitude m_b=5.2 earthquake in western Turkey are shown. Pulse width was measured from the record with cut-off period 7 seconds. The long and short vertical lines show the manually adjusted times t_1 and t_2. The pulse, limited by times t_s and t_e, is shown as the top trace. The computed pulse width is 1.28 seconds, giving a cut-off/width ratio of 5.5 which according to the discussion in chapter II indicates that pulse width was not reduced by cut-off. The duration of the pulse is 2.24 seconds. The shown event illustrates an interesting phenomenon, the pulse has two maxima. Incidentally, when the cut-off period decreases the two maxima separate to two pulses. A pulse width measurement from the trace with cut-off 2.5 would give too small pulse width, in itself a natural result from too small true width/cut-off ratio, but in this case unobservable since the minimum in the pulse disrupts the rule-of-thumb given in chapter II. Even the underestimated pulse width (0.45 s) falls within the earthquake population in the classification diagram V.2, however.

Pulse widths measured for the first 84 events of the LASA data tape created by Lacoss[24] are shown in figure V.2. The

rule that a pulse width is measured first and the nature of the event checked only afterwards was strictly obeyed. In addition a few confidence limits and the earthquake and explosions mean square pulse width lines, computed from <u>independent</u> samples of pulse widths measured from NORSAR records, are drawn to fig. V.2.

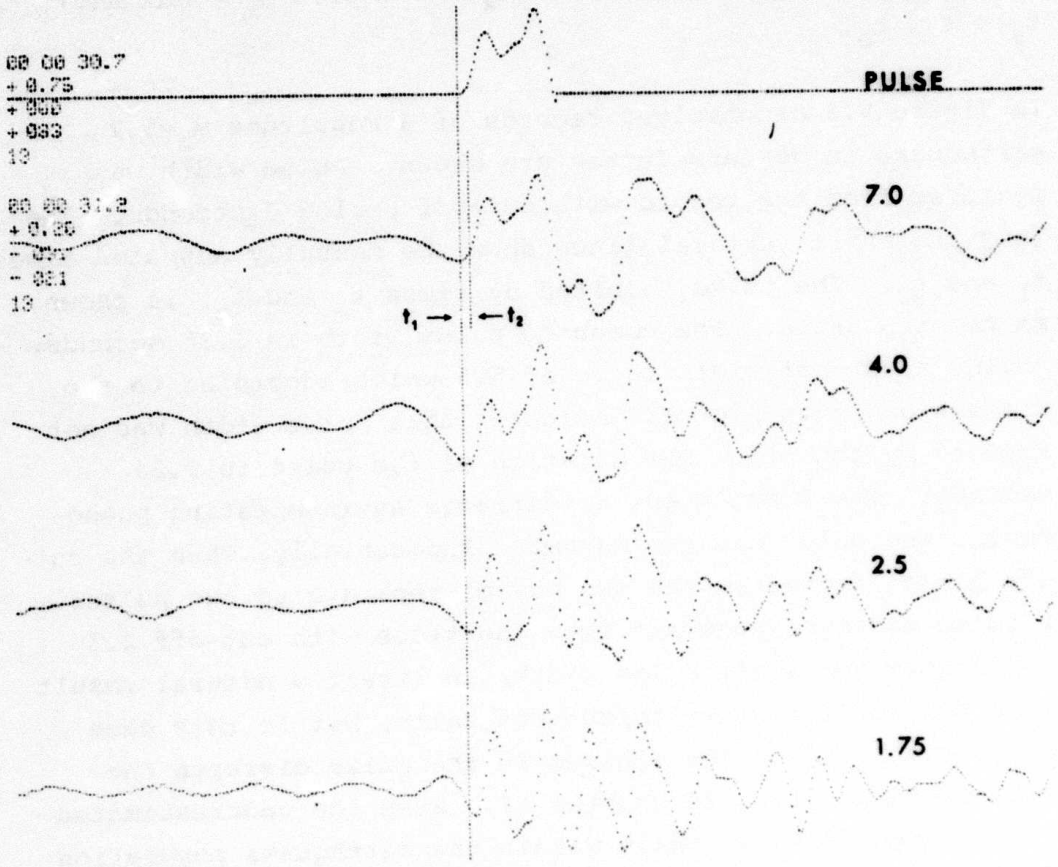

Fig. V.1. Deconvolved records from A m_b=5.2 earthquake in western Turkey, recorded by LASA. The figures at right margin give the cut-off period for each trace. The top trace shows the semi-automatically selected pulse from the record with cut-off 7.0. The times t_1 and t_2 were manually set.

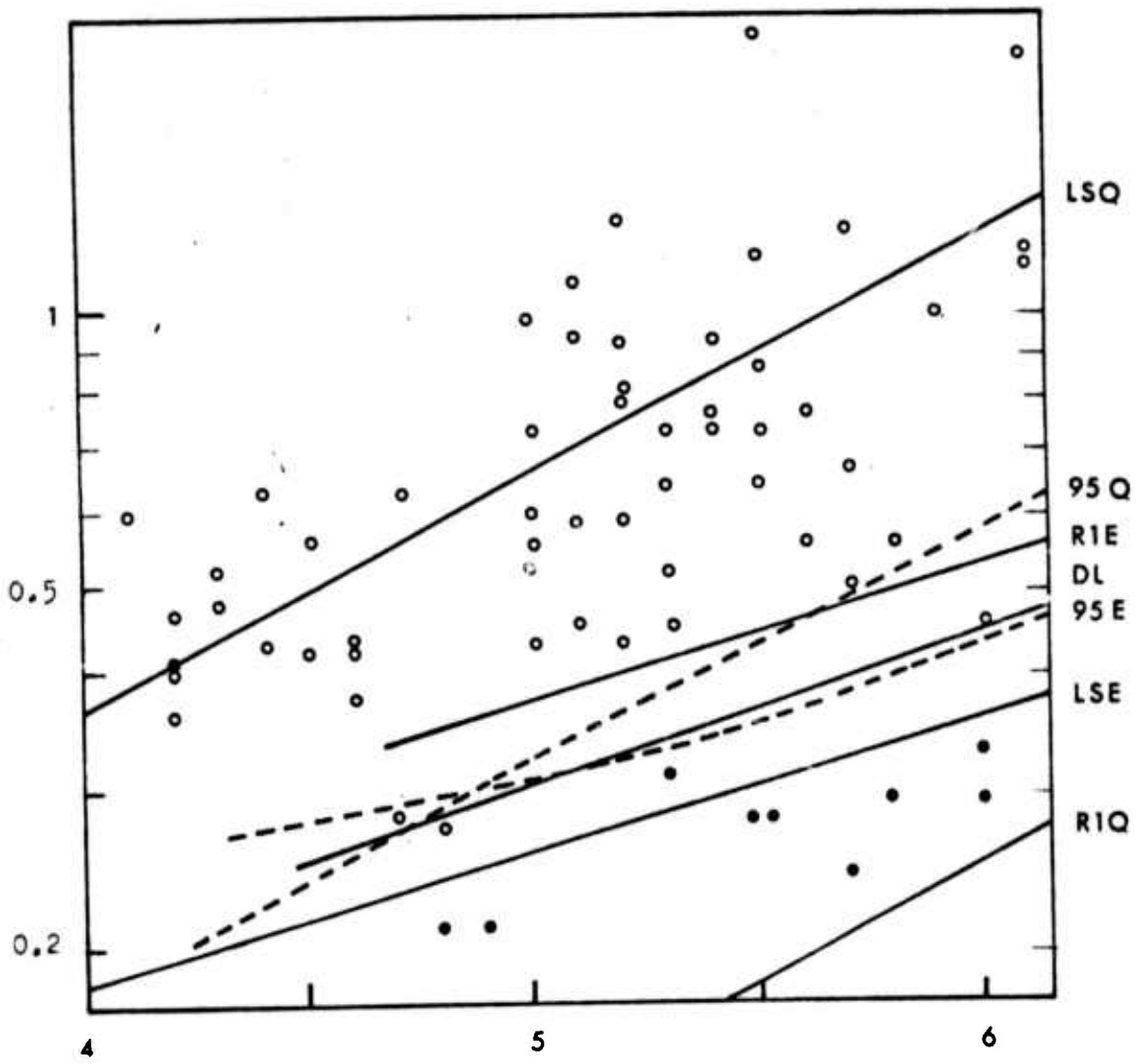

Fig. V.2. Pulse widths measured for earthquakes (open circles) and explosions (filled circles) recorded by LASA. The statistics plotted to the figure are derived from independent earthquake and explosion populations recorded by the NORSAR array. LSQ=least squares line for earthquakes. 95Q=95% confidence limit for a single earthquake pulse width, R1Q=99% confidence limit for detecting outliers from the earthquake population. LSE, 95E, R1E corresponding quantities for explosions. DL=preliminary decision line.

The sample of earthquakes used in computing the statistics is the set (5) of chapter VI, it consists of 53 quakes. The explosion sample consists of 17 Eastern and Central Kazakh shots, the NTS shots were excluded in computing the statistics, since they seemed to belong to a different population. No NTS shots are included in the LASA data tape. It is necessary later to unify all observed explosions under a single description, to be more confident that no anomalous explosion populations will appear, to which our expectations do not hold.

The computed statistics are[23]: (1) The least squares lines for NORSAR-recorded earthquakes (LSQ) and explosions (LSE). (2) The one-sided 95 % confidence limits for a single sample, lower limit for earthquakes (95Q), upper limit for explosions (95E). (3) The 99 % confidence limits for rejecting outliers from the explosion population (R1E) and from earthquake population (R1Q). A preliminary decision line (DL) is also drawn to the figure. It divides the distance between the least-square lines in the ratio of the residual RMS values of explosions and earthquakes.

The small scatter of the original Kazakh explosion pulse width data at NORSAR is reflected in the outlier test for explosions, which suggests all except 3 of the quakes not to belong to the explosion population, with a 99 % confidence. On the contrary the large scatter of earthquake pulse widths causes that none of the explosions when treated singly is suggested to be an outlier from the earthquake population at the same level of confidence. It is thus easier to identify quakes than explosions.

One of the earthquakes falls out of the 95 % confidence region for single earthquakes, and into the 95 % confidence region for explosions. That is a deep shock in Rumania (depth 151 km). There are other deep shocks with normal pulse widths, however. Two other earthquakes are marginal, they are shallow shocks. Results are summarized in table V.1.

Table V.1. Results of the discrimination experiment

source type	classified as: explosion	earthquake	marginal	rejected	total
EXPLOSION	10	0	0	1	11
EARTHQUAKE	1	56	2	14	73

The one rejected explosion was clipping. In figure V.3 are shown the deconvolved records of 9 explosions, and of the three earthquakes not classified as earthquakes. We think that all of these quakes are in some way different from the explosion records. Q/1 is the deep shock, it has no pP reflection following the primary pulse, as all the explosions have. Q/2 is the most problematic of all. It is a shallow shock with magnitude m_b=4.7 at Kuriles, under the ocean. A secondary negative impulse appears, resembling the pP reflection from explosions. The later reverberations of the signal are however larger and with a longer duration than for any of the explosions. The S/N ratio is bad. The event Q/3 is a m_b=6 shock in SE Europe. Apparently we are measuring a small precursor of a large and complex shock. The appearance of the record is clearly not explosion-like.

The original beam traces of the same 12 events are shown in figure V.4. The amplitude gain of each record is random.

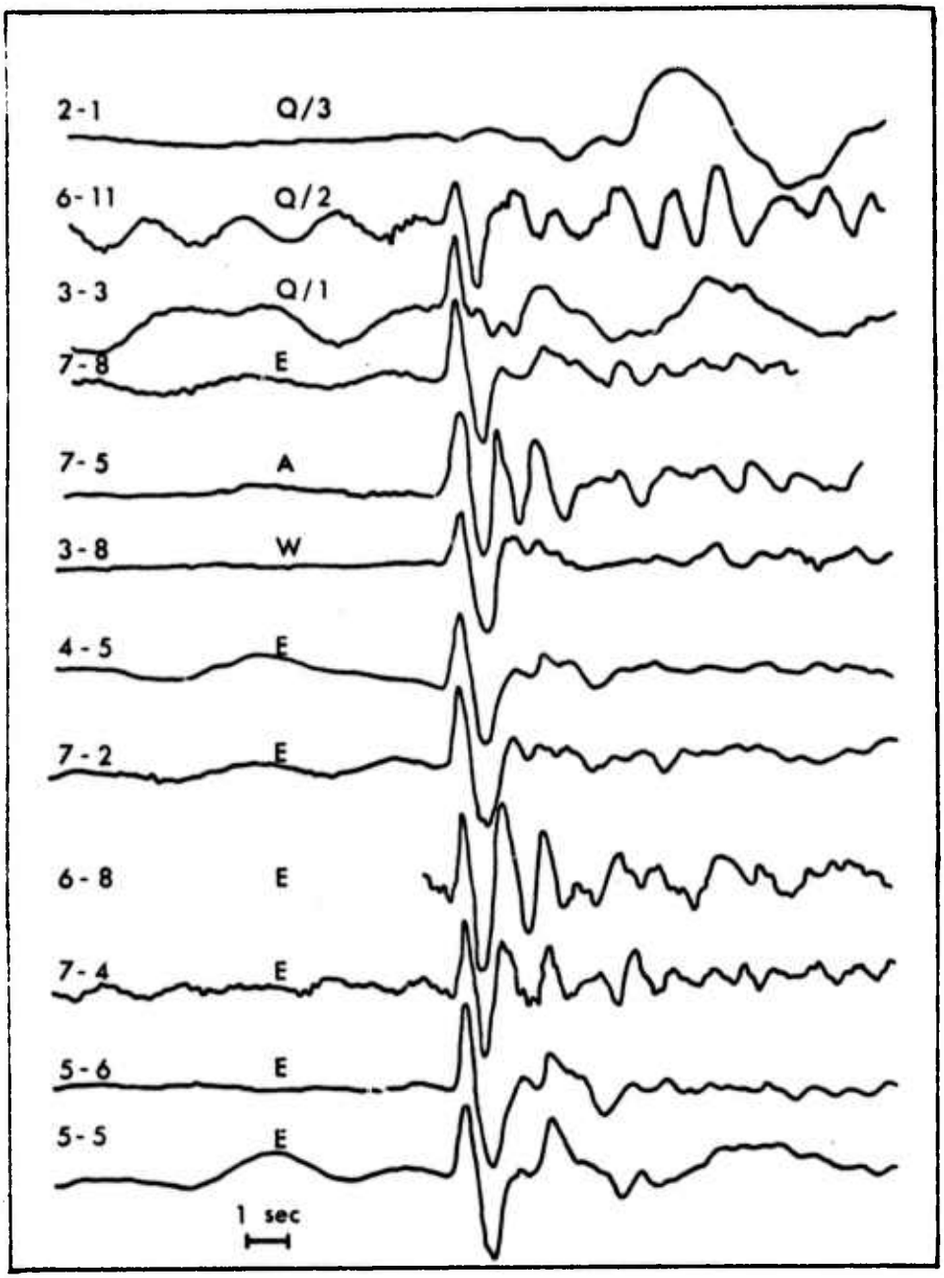

Fig. V.3. Deconvolved records for the explosions and the three earthquakes not classified as earthquakes. E=Eastern Kazakh, W=Western Kazakh, A=Aleutians. Q stands for quake. Code numbers refer to appendix. Amplitudes are normalized.

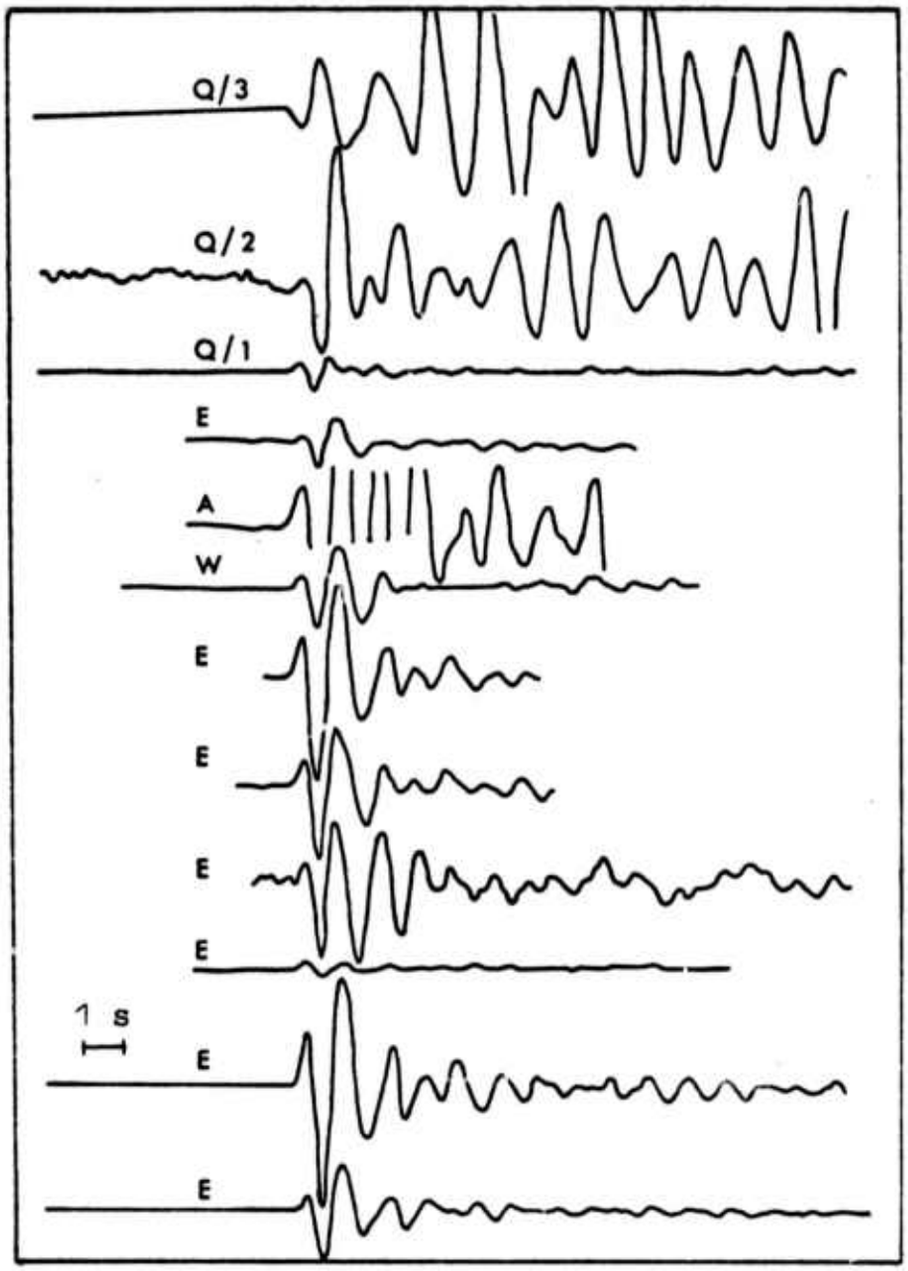

Fig. V.4. Original LASA beam traces of the same events as displayed in previous figure. Amplitude gains are random.

The polarity of the event Q/2 is somewhat uncertain, during analysis it was decided to be positive. A supplement to the pulse width discriminant is the polarity, since the determination of the width requires the pulse polarity to be first determined. At distances above 30 degrees all explosions from which the pulse width can be determined display unmistakably compressions. For earthquakes also dilatations are observed.

Next the 95 % one-sided confidence limits for a single sample, the least square lines and the preliminary decision line are computed from the LASA event sample itself. These are thus statistics which can be used in classifying new LASA-recorded events. They are shown in figure V.5. The data points are also plotted to the figure.

In table V.2 are shown the number of events accepted to the "measurable" category and the total number of analysed events, and the percentage of accepted measurements in several magnitude categories.

Table V.2. Statistics on measurement capability

m_b class	total	accepted	acc.%
4.0-4.9	33	21	63%
5.0-5.9	43	42	98%
over 6.0	7	6[1]	

1) one of the large explosions clips.

The pulse width measurements can often be extended to such explosions, for which M_s is not measurable and m_b-M_s classifier cannot be used.

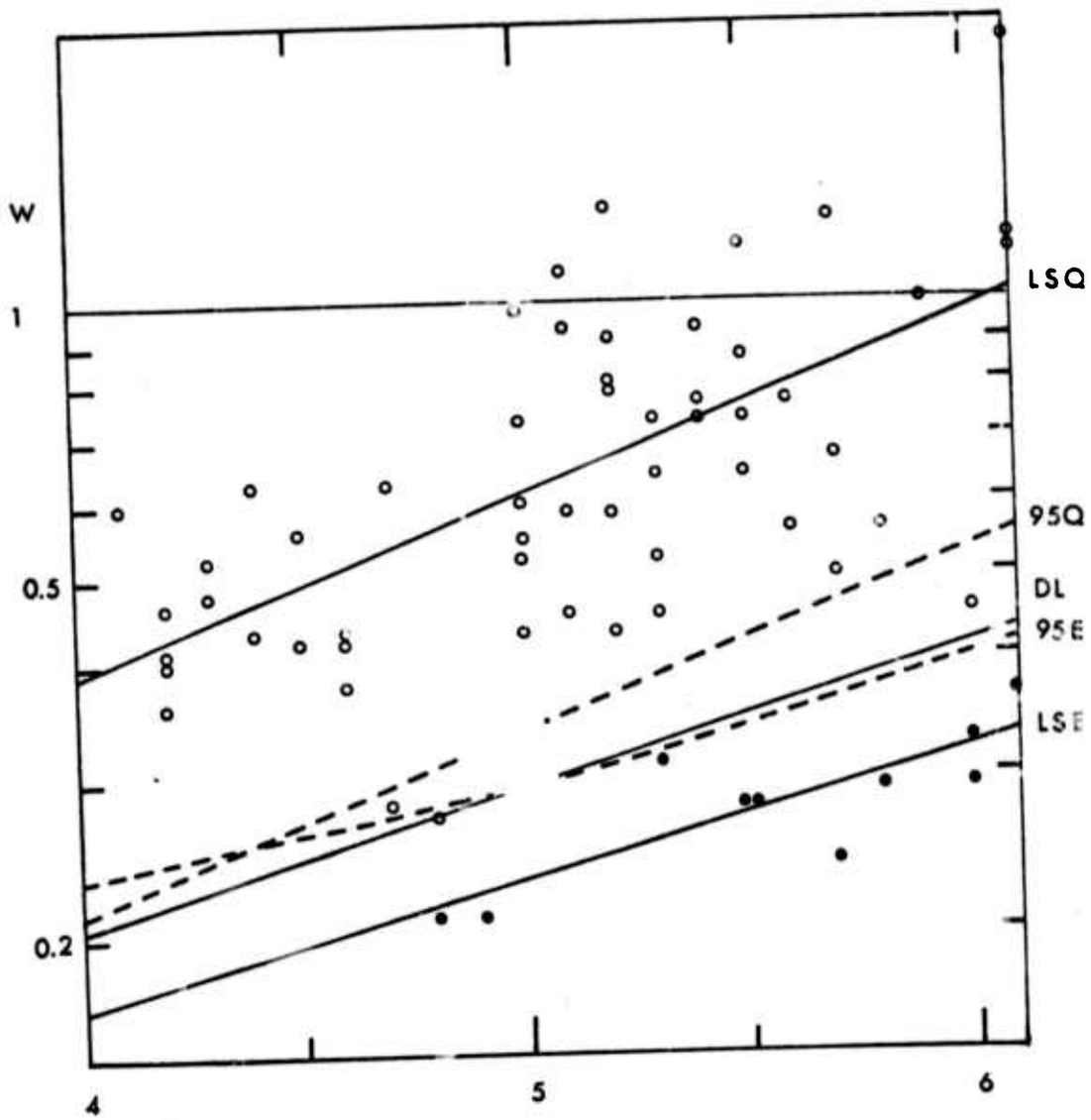

Fig. V.5. Statistics computed from the LASA pulse width data sample analysed in this chapter. Symbols are the same as in figure V.2. The width measurements are again plotted. These statistics were not used in the discrimination experiment.

VI. IMPLICATIONS TO OTHER DISCRIMINANTS

The knowledge on source duration and P-wave attenuation which has been achieved in the previous chapter may be applied to exptrapolate and predict values of such other discriminants which are influenced by these quantities.

The LTM discriminant[12] measures the amount of P-wave high frequency energy relative to the low frequency energy. The normalized third moment of the noise-corrected power spectrum around the frequency origin is computed. By defining the quantities t^* and f_o, and applying Brune and the HSB model for earthquakes and explosions, respectively, sets of predicted spectra were computed. These were then multiplied by the NORSAR amplitude response and LTM values were computed.

In figure VI.1 the results are compared with earthquakes and explosions in Asia and North America. t^* values from figure III.1, earthquake f_o values derived from figure IV.2 and explosion f_o values derived from figure V.2 using (4.2) were used. Agreement is acceptable for earthquakes and explosions in Central Asia, Turkey, and Sakhalin. The predicted curves lie too high for North America ($t^*=0.5$) and too low for Kuriles ($t^*=0.2$). It is again observed that even using our estimated attenuation figures, events in North America have still weaker high frequency energy than expected, and events in Kuriles have still stronger.

As mentioned in chapter III the probable cause for these phenomena is a spectral model which does not quite well fit

reality. One possible consequence is that attenuation on North America-NORSAR paths is underestimated and on Kuriles-NORSAR path overestimated. Another observation is that the observed earthquake LTM values decrease more steeply with increasing magnitude than the predicted values.

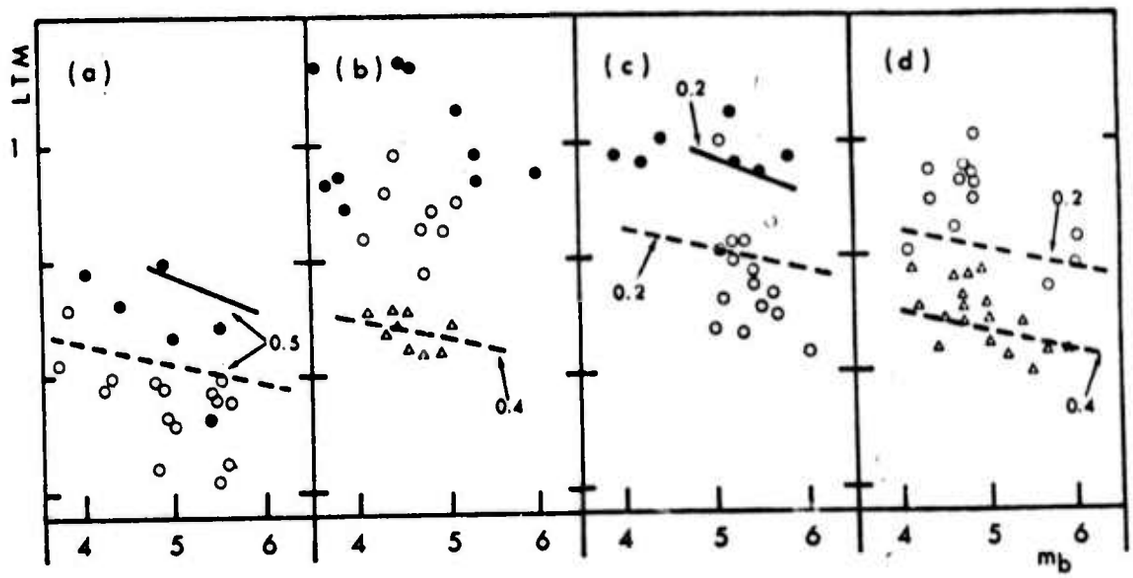

Fig. VI.1. At NORSAR observed LTM values from ref. 12 compared with predicted values. Explosion and earthquake observations are plotted with filled and open symbols, respectively. Continuous and broken lines denote predictions for explosions and quakes. (a) Events in south-western North America. (b) Explosions in western Russia, earthquakes in southern Greece (circles) and Turkey (triangles). (c) Events in Central Asia. (d) Earthquakes at Kuriles (circles) and Sakhalin (triangles). Almost all of the events in the figure are shallow, and none is deeper than 100 km.

Next it will be attempted to combine our results with m_b-M_s observations. The magnitude M_s is first derived. The amplitude of Rayleigh waves at period 20 seconds is given as

$$A_{R20} = \frac{20}{2\pi} P_o \, D_{R20}(\Delta) |W_R(h,S,E)|$$

for a step source time function. P_o is seismic source moment, $D_{R20}(\Delta)$ is the influence of distance on amplitude, W_R is the effect of source depth h, mechanism S and Earth structure E. Douglas, Hudson and Kembhavi[26] showed that a separation of factors in this way is possible. Since M_s is defined

$$M_s = \log (A_{R20}) + Q_R(\Delta)$$

where

$$Q(\Delta) + \log (D_{R20}(\Delta)) = e_R$$

e_R being a constant, related to the origin of the M_s scale, we get for M_s

$$M_s = \log \frac{20}{2\pi} + \log P_o + e_R + \log |W_R(d,S,E)|$$

For the m_b magnitude one can give the following derivation. The amplitude spectrum of a P wave is

$$A_p(f) = F(f) \, P_o \, D_P(\Delta,h,E) \exp(-\pi f t^*) |W_p(S,E)|$$

where F(f) is the amplitude spectrum of the source time function, D_P stands for geometrical attenuation and the

effect of the free surface at receiver end, t^* is the ray path attenuation and W_p gives the effect of the properties of the supposed homogeneous medium surrounding the source, and of the source radiation pattern, assumed to influence only the amplitude. Only the very inifial part of the wave is considered, thus the pP and other reflections can be neglected.

The recorded amplitude spectrum T(f) is the product of $A_p(f)$ and instrument response. It has a roughly Gaussian shape with maximum amplitude A_m at frequency f_m, and width c. Such a spectrum yields on Fourier transform[9] a wave packet with amplitude $A = A_m c/\sqrt{\pi}$ and frequency f_m. From inspection of recorded spectra it was concluded that a relationship $c = f_m$ roughly describes the spectra. Since the distance correction in m_b computation compensates for the $D_p(\Delta,h,E)$, we get for m_b

$$m_b = \log F(f_m) + \log P_o + e_p - 0.43\, t^* \pi f_m + \log|W_p|$$

$$+ 2 \log f_m - \log \sqrt{\pi}$$

and for the difference $m_b - M_s$

$$m_b - M_s = \log F(f_m) - 0.43\pi t^* f_m + 2 \log f_m + C$$

where all the factors which do not depend on magnitude are lumped together to a constant C. They are either constants or random quantities with some expected values.

Using the same source spectral models and f_o/m_b relationships

as in computation of the predictions for the LTM, we get for $m_b - M_s$ as a function of m_b the curves which are shown in figure VI.2, together with observations by Bungum[27] and by Filson and Bungum[28]. The undefined constant C is determined so that both of the explosion and earthquake curves pass through the observed points.

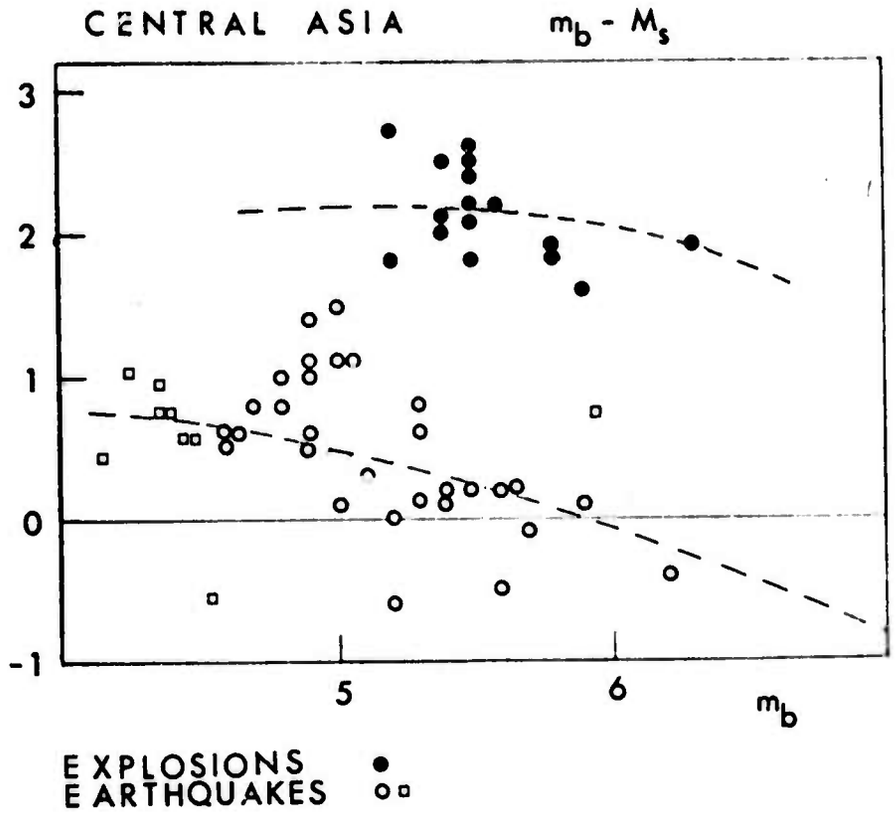

Fig. VI.2. $m_b - M_s$ values of explosions in Eastern Kazakh and earthquakes in Central Asia. Broken lines give the expected shapes of $m_b - M_s$ as a function of m_b, levels of the curves in the vertical direction are determined by the observations. m_b is measured only at NORSAR for events with square symbols. Earthquakes are plotted with open, explosions with filled symbols.

The essential feature of the two curves in figure VI.2 is that they approach each other as magnitude decreases. The question whether they will converge to one at very small magnitudes was treated by Douglas, Hudson and Kembhavi[29], who showed that when the events are so small that the source time function appears step-like also in the frequency range of the short period sensor response, the difference $m_b - M_s$ depends on which of the following two factors dominates: (a) The stronger shear-wave generation of the double-couple earthquake source gives for the quakes larger M_s values than for the explosions, and (b) the larger depth of earthquakes decreases the earthquake M_s values relative to explosions.

The contents of this chapter has also been discussed in reference 30.

VII. SUMMARY AND CONCLUSIONS

The practical aspects of deconvolution of a recorded trace to a record of earth displacement are investigated and it is concluded that the area of a unidirectional wave pulse can be determined with distortion less than 10 % if the pulse lenght/ cut-off period ratio is less than 0.35. The cut-off refers here to the filtering away of the lowest frequency components of the deconvolved record, containing only instrument noise. E.g. a pulse of 2 seconds in lenght requires that frequencies down to 0.175 hz be included in synthesis of the deconvolved trace, using FFT methods.

The pulse lenght was defined as the time interval between the pulse onset and the moment when the displacement returns back to its pre-pulse value. The pulse <u>width</u> was defined as the pulse area/height ratio. Pulse width is usually half of its lenght. The pulse width is naturally influenced by the amount of attenuation. It is possible to correct for some attenuation. A change of 0.2 in attenuation parameter t^* produces a change of 20-30 % in pulse width. For explosions at distances less than 30 degrees from NORSAR often no distinct pulse was observed. This is interpreted as caused by multipathing in the upper mantle.

The common spectral model consisting of a flat low-frequency model, a corner frequency f_o, a high-frequency constant slope of f^{-n} and an attenuation factor $\exp(-\pi f t^*)$ was fitted to 60 explosion and earthquake spectra, grouped regionally. The t^*-values from all studied Asian locations to NORSAR were

observed to be less than 0.4. The smallest observed attenuation (on path Kuriles-NORSAR) has t^*=0.1 or 0.2, depending on assumptions on source spectrum. Values (under different assumptions on source models) for the ray paths from Central Asia to NORSAR range from 0.15 to 0.25 in t^*, corresponding to a mean Q equal or greater than 2000. Ray paths from SW North America to NORSAR have a larger attenuation than any ray path under Asia.

The simple spectral model does not probably quite well describe reality, as evidenced by an unexpected correlation among the derived parameters, and in some cases by excessive corner frequencies, when compared to pulse widths measured by deconvolution. A probable deficiency is the existence of only one corner frequency in the model, while actually several corners may appear, separated by intermediate spectral slopes[16]. Both of the values n=2 and n=3 were tried, no clear preference for either one was deduced. Corner frequencies could be estimated simultaneously with a regional average t^*, but with a considerable scatter. Fitting of a spectral model to explosion spectra succeeded only if a very wide frequency range (up to 6 hz) could be used.

Pulse widths were measured for the same events, spectra of which had been studied. Pulse widths, as also corner frequencies, are correlated with event magnitude. Explosions have pulse widths about half of those of earthquakes with same magnitude. The NTS explosions recorded at NORSAR seem to have excessive pulse widths, and require an attenuation correction larger than that predicted by the spectral measurements to be reduced to the same pulse width as the E. Kazakh shots. It is important to bring all explosions under a same statistical,

preferably Gaussian, population, to be able to set predictions and statistical limits independently of region. In the following table observed average time constants of seismic events are given

Table VII.1. Time constants. W=pulse width (s), D=source duration, f_o=corner frequency (hz)

	earthquakes			explosions	
m_b	W	D	f_o	W	f_o
4.0	0.40	0.8	0.8		
5.0	0.65	1.2	0.5	0.25	1.3
6.0	1.1	2.2	0.3	0.32	1.0

The pulse width seems to function as a discriminant. It is the author's opinion that after the m_b - M_s discriminant, the pulse width is best in separation capability and applicability. It was tested to an independent sample of earthquakes and explosions recorded at LASA. A benefit of the deconvolution procedure is that after measuring the pulse width, one is still left with the deconvolved seismogram which frequently still contains useful information and may alert the observer in case of multiple events etc. Deconvolution could be a standard procedure in a monitoring scheme since it, as broad-band seismograms in general, displays waveform information easily.

APPENDIX

In the following table the first 84 events on a tape containing LASA beams and compiled by R.T.Lacoss and J.R.Filson (Lincoln Laboratory, M.I.T.) are listed. The order of the events is the same as on the tape, the epicentral information is from the Bulletin of the International Seismological Centre, or in a few cases from LASA, in these cases the location is given only in full degrees. For each event is given the pulse width measured by the author (P.W.) and the low-frequncy cut-off period in seconds (C-O.). When the cut-off/width ratio is less than 4 and according to the discussion in Chapter II one may assume that the measured pulse width is less than the true pulse width, the word "REDUCED" is written.

FILE 1

DATE	TIME	COORDINATES		DEPTH	MB	P.W.	C-O.	COMMENTS
67-04-01	12-23-35	45.7N	151.8E	40	5.9	0.99	(7.0)	
66-12-07	17-17-42	44.3N	151.7E	26	5.8	0.55	(7.0)	
67-10-07-08-28-01		49.2N	156.3E	33	5.3	0.45	(4.0)	
67-11-01-16-30-57		48.3N	154.4E	40	5.5	0.64	(7.0)	
68-04-08	10-10-24	41.1N	19.9 E		4.2	----	(2.0)	
68-04-15	01-39-04	41 N	22 E		4.1	----	(2.0)	
68-04-11	06-46-27	42.5N	131.0E	511	5.0	0.52	(10.)	
68-04-17-19-14-00		53.9N	160.1E	33	4.1	----	(2.0)	
68-01-27	02-21-58	40.5N	72.1E	52	4.8	----	(1.7)	LASA MB
68-01-18	21-57-03	82.3N	119.5E	48	4.5	0.62	(1.7)	REDUCED
68-01-29	10-42-08	43.2N	147.2E	41	5.2	0.80	(4.0)	
68-01-29	11-25-24	43.6E	147.2E	33	4.4	0.36	(2.0)	

FILE 2

67-11-30	07-23-51	41.5N	20.5E	29	6.0	0.45	(10.)	
67-12-23	16-04-38	48.2N	157.3E	26	5.1	0.45	(7.0)	
67-05-25	18-52-17	46.0N	143.0E	325	4.8	----		
66-08-19	12-22-09	39.2N	41.7 E	26	6.1	1.94	(7.0)	
68-04-17	13-11-26	36.4N	71.5 E	113	5.2	0.91	(7.0)	
68-04-18	03-08-02	41.3N	20.3E	33	4.4	0.43	(2.5)	
68-04-21	14-44-06	54.9N	161.5E	28	4.6	0.42	(1.7)	
68-04-17	09-12-04	35.2N	3.7W	16	5.0	0.54	(7.0)	
68-01-29	11-29-01	42.7N	147.6E	33	4.2	0.40	(1.7)	
68-01-29	11-36-37	43.1N	146.7E	77	4.2	0.46	(1.7)	REDUCED
68-01-29	11-43-59	43.4N	147.3E	33	5.1	1.08	(3.0)	REDUCED
68-01-29	12-07-08	43.2N	147.3E	33	5.0	----	(1.7)	

FILE 3

67-03-25	22-47-58	45.5N	151.4E	41	5.5	2.0	(7.0)	
66-05-20	11-44-29	55.0N	165.7E	46	5.2	0.78	(7.0)	
66-12-14	14-49-59	45.6N	26.4E	158	4.8	0.27	(4.0)	
67-01-05	10-07-58	39.4N	72.9E	11	5.3	0.64	(2.5)	REDUCED
68-04-23	02-43-45	38.7N	70.6E	29	4.8	----	(1.7)	
68-04-23	22-30-27	34.6N	8.9E	33	4.2	0.41	(1.7)	
66-10-27	05-57-58	73.4N	54.8E	0	6.3	clips		
68-07-01	04-02-02	47.9N	48.0E	33	5.5	0.28	(4.0)	
68-01-30	01-48-29	43.3N	147.7E	33	5.1	0.58	(1.5)	REDUCED
68-01-29	17-14-06	43.4N	147.3E	33	4.5	----	(1.7)	
68-01-29	16-42-50	43.5N	147.2E	36	5.7	1.24	(4.0)	REDUCED
68-01-29	16-04-12	43.1N	146.9E	40	4.6	0.43	(2.5)	LASA MB

FILE 4

DATE	TIME	COORDINATES		DEPTH	MB	P.W.	C-O.	COMMENTS
67-01-11	11-20-46	34.1N	45.7E	34	5.6	0.77	(7.0)	
67-04-01	05-57-09	46.3N	152.0E	40	5.5	0.86	(4.0)	
67-01-20	01-57-23	48.0N	102.9E	33	6.1	1.17	(7.0)	
66-11-21	12-19-27	46.7N	152.5E	40	5.6	0.56	(4.0)	
66-03-20	05-49-58	49.7N	78.0E	0	6.0	0.33	(7.0)	
67-04-07	18-33-31	37.4N	36.2E	39	5.0	0.96	(4.0)	
67-01-05	23-58-21	48.1N	102.9E	33	5.4	0.73	(4.0)	
66-05-07	13-08-16	37.8N	27.9E	12	5.2	1.28	(7.0)	
68-01-30	08-17-32	36.4N	70.7E	205	5.2	0.43	(2.5)	
68-01-30	01-30-13	43.3N	146.8E	12	5.3	0.73	(4.0)	
68-02-06	10-30-34	54.9N	162.1E	33	4.2	0.36	(1.7)	
68-02-07	01-22 06	30.9N	80.3E		4.7	----	(1.7)	

FILE 5

67-04-01	14-00-34	45.8N	151.7E	23	5.4	0.87	(4.0)	
67-04-27	23-15 20	41.7N	82.3E	33	5.0	0.59	(2.5)	
67-05-27	01-42-47	39.9N	77.3E	33	5.4	0.77	(1.7)	REDUCED
67-05-27	19-05-48	36.1N	77.8E	35	5.4	0.93	(4.0)	
67-04-20	04-07-58	49.7N	78.1E	0	5.7	0.24	(7.0)	
67-02-26	03-57-58	49.8N	78.1E	0	6.0	0.29	(4.0)	
66-06-04	05-11-54	36.3N	70.8E	207	5.7	0.67	(7.0)	
66-10-29	02-39-29	39.2N	21.2E	20	5.7	0.49	(7.0)	
68-02-07	22-22-20	36.7N	26.8E	161	5.0	0.59	(7.0)	
68-02-13	07-42-16	38.4N	73.2E	33	4.3	0.47	(1.5)	REDUCED
68-03-17	17-46-53	79.9N	140.0E	33	4.5	0.56	(1.7)	REDUCED
68-02-22	12-34-11	41.5N	20.0E	33	4.1	----	(1.5)	LASA MB

FILE 6

67-06-07	18-16-31	47.6N	155.4E	29	5.2	0.58	(7.0)	
67-10-05	15-55-03	45.4N	150.7E	33	5.3	0.52	(2.5)	
67-12-14	18-25-17	54.6N	160.4E	33	5.5	0.73	(7.0)	
67-12-16	20-53-58	51.2N	157.7E	24	5.5	1.17	(7.0)	
67-01-18	05-34-33	56.6N	120.8E	11	6.1	1.13	(7.0)	
68-05-11	12-12-41	41.0N	49.8E	16	5.0	0.43	(2.5)	
68-05-13	02-46-36	43.5N	40.3E	5	5.1	0.93	(7.0)	
66-08-19	03-53-01	50.4N	77.9E	0	4.8	0.21	(1.7)	
68-02-22	12-22-50	41.7N	20.1E	46	4.4	0.63	(2.5)	LASA MB
68-02-22	09-55-47	41.8N	21.5E		4.1	0.60	(1.5)	REDUCED
68-01-11	18-08-38	46.4N	153.3E	50	4.7	0.23	(1.5)	
68-01-08	09-28-04	49.7N	155.9E	63	4.3	0.52	(1.7)	REDUCED

FILE 7

DATE	TIME	COORDINATES	DEPTH	MB	P.W.	C-O.	COMMENTS
67-12-19	03-37-43	38 N 72 E		4.7	0.63	(1.7)	LASA MB
65-11-21	04-57-58	49.8N 78.1E	0	5.8	0.29	(2.5)	
67-10-30	06-03-58	49.8N 78.1E	0	5.5	0.28	(4.0)	
66-05-07	03-57-58	49.7N 77.9E	0	4.9	0.21	(1.7)	
65-10-29	21-00-00	51.4N 179.2E	0	6.1	0.37	(4.0)	
67-04-07	19-39-13	47.0N 146.0E	296	5.0	0.74	(4.0)	
68-06-24	18-2[illegible]-46	40.4N 48.8E	33	4.6	0.38	(1.7)	
68-06-11	03-05-58	49.3N 78.2E	0	5.3	0.31	(2.5)	
68-01-07	21-38-52	45.9N 150.7E	111	4.5	0.42	(1.7)	
68-01-07	18-45-48	55 N 164 E		4.1	0.48	(1.7)	REDUCED
68-01-07	07-42-04	43.7N 134.0E	378	4.5	----	(1.7)	
68-01-05	02-51-33	88 N 50 E		4.0	0.50	(1.7)	REDUCED

REFERENCES

1. Randall, M.J., "Spectral peaks and earthquake source dimension", Jour. Geophys. Res., Vol. 78, pp. 2609-2611 (May 1973).

2. Haskell, N.A., "Analytic approximation for the elastic radiation from a contained underground explosion", Jour. Geophys. Res., Vol. 72, pp. 2583-2587 (May 1967).

3. Randall, M.J., "Seismic radiation from a sudden phase transition", Jour. Geophys. Res., Vol. 71, pp. 5297-5302 (November 1966).

4. Bogert, R.P., M.J. Healy and J.W. Tukey, "The frequency analysis of time series for echoes", Time Series Analysis, edited by M. Rosenblatt, John Wiley & Sons, Inc. (1963).

5. Savage, J.C., "Radiation from a realistic model of faulting", Bull. Seism. Soc. Am., Vol. 56, pp. 577-592 (April 1966).

6. Carpenter, E.W., "Absorption of elastic waves - an operator for a constant Q mechanism, United Kingdom Atomic Energy Authority, AWRE Report D-43/66 (October 1966).

7. Frazier, C.W., "Observations of pP in the short-period phases of NTS explosions recorded at Norway", Geophys. J.R. astr. Soc., Vol. 31, pp. 99-109 (1972).

8. Aki, K., "Scaling law of seismic spectrum", Jour. Geophys. Res., Vol. 72, pp. 1217-1231 (February 1967).

9. Randall, M.J., "The spectral theory of seismic sources", Bull. Seism. Soc. Am., Vol. 63, pp. 1133-1144 (June 1973).

10. Berckhemer, H. and K.H. Jacob, "Investigation of the dynamical process in the earthquake foci by analyzing the pulse shape of body waves", Final Sci. Rept., 1 June 1964 to 31 December 1967, Contract AF 61(052)-801, Inst. of Meteor. & Geophys., Univ. of Frankfurt (1968).

Burdick, L.J. and D.V. Helmberger, "Time functions appropriate for deep earthquakes", Bull. Seism. Soc. Am., Vol. 64, pp. 1419-1428 (October 1974).

11. Massé, R.P. and S.S. Alexander, "Compressional velocity distribution beneath Scandinavia and Western Russia", Geophys. J.R. astr. Soc., Vol. 39, pp. 587-602 (1974).

12. Noponen, I., "Compressional wave power spectrum from seismic sources", Sci. Rept. No. 1, June 30, 1972 to June 29, 1973, Grant OSR-72-2377, University of Helsinki (October 1973).

13. Haskell, N.A., "Total energy and energy spectral density of elastic wave radiation from propagating faults", Bull. Seism. Soc. Am., Vol. 54, pp. 1811-1841 (December 1964).

14. Brune, J.N., "Tectonic stress and the spectra of seismic shear waves from earthquakes", Jour. Geophys. Res., Vol. 75, pp. 4997-5009 (September 1970).

15. Savage, J.C., "Relation between P- and S-wave corner frequencies in the seismic spectrum", Bull. Seism. Soc. Am., Vol. 64, pp. 1621-1627 (December 1974).

16. Savage, J.C., "Relation of corner frequency to fault dimensions", Jour. Geophys. Res., Vol. 77, pp. 3788-3795 (July 1972).

17. Frazier, C.W. and J.R. Filson, "A direct measurement of the Earth's short period attenuation along a teleseismic path", Jour. Geophys. Res., Vol. 77, pp. 3782-3787 (1972).

18. Seggern, D. von and R. Blandford, "Source time functions and spectra for underground nuclear explosions", Geophys. J.R. astr. Soc., Vol. 31, pp. 83-97 (December 1972).

19. Burridge, R. and L. Knopoff, "Body force equivalents for seismic dislocations", Bull. Seism. Soc. Am., Vol. 54, pp. 1875-1888 (December 1964).

20. Müller, G., "Seismic moment and long-period radiation of underground nuclear explosions", Bull. Seism. Soc. Am., Vol. 63, pp. 847-857 (June 1973).

21. Randall, M.J., "Low-frequency spectra in seismic waves from explosions", Geophys. J.R. astr. Soc., Vol. 32, pp. 387-388 (1973).

22. Douglas, A., J.B. Young and J.A. Hudson, "Complex P-wave seismograms from simple earthquake sources", Geophys. J.R. astr. Soc., Vol. 37, 141-150 (1974).

23. Acton, F.S., "The classical model", Chapter 2, Analysis of Straight-Line Data, Dover publ., Inc. (1966).

24. Lacoss, R.T., "A large-population LASA discrimination experiment", Technical Note 1969-24, Lincoln lab., M.I.T. (April 1969).

25. Chinnery, M.A. and R.G. North, "The moment-M_s relationship, and the frequency of large earthquakes", Semiannual Tech. Summary Rept., 30 June 1974, Lincoln Laboratory, M.I.T. (June 1974).

26. Douglas, A., J.A. Hudson and V.K. Kembhavi, "The analysis of surface wave spectra using a reciprocity theorem for surface waves", Geophys. J.R. astr. Soc., Vol. 23, pp. 207-223 (1971).

27. Bungum, H. and I. Noponen, "m_b:M_s at NORSAR", NORSAR Semiannual Tech. Rept., 1 January - 30 June 1974, ed. by H. Bungum, Kjeller (September 1974).

28. Filson, J. and H. Bungum, "Initial discrimination results from the Norwegian seismic array", Geophys. J.R. astr. Soc., Vol. 31, pp. 315-328 (December 1972).

29. Douglas, A., J.A. Hudson and V.K. Kembhavi, "The relative excitation of seismic surface body waves by point sources", Geophys. J.R. astr. Soc., Vol. 23, pp. 451-460 (1971).

30. Noponen, I., "Event identification capabilites of NORSAR", Proceedings from NATO A.S.I. "Seminar on exploitation of seismograph networks, Sandefjord, Norway, 1974 (to be published).